The International Journal of Advanced Manufacturing Technology (2019) 104:33–61
https://doi.org/10.1007/s00170-019-03682-6

ORIGINAL ARTICLE

A review on material fracture mechanism in incremental sheet forming

Sheng Ai[1] · Hui Long[1]

Received: 21 November 2018 / Accepted: 31 March 2019 / Published online: 10 May 2019

Abstract

In incremental sheet forming (ISF), including single point incremental forming (SPIF) and double side incremental forming (DSIF), the material formability can be significantly enhanced when compared with conventional sheet forming processes. The material deformation in ISF is far more complicated because of the combined material deformation under stretching, bending, shearing, and cyclic loading, with an additional effect of compression in DSIF. Despite extensive investigation on material deformation during ISF, no theory has yet been widely agreed to explain different types of the material fracture behavior observed in ISF experiments. This paper presents a comprehensive review on the formability enhancement in ISF and proposes possible fracture mechanisms explaining the different types of fracture behavior observed in the experimental investigations. Discussions are presented to outline the current research progress and possible solutions to overcome the current ISF process limitations because of the material processing failure due to fracture.

Keywords ISF · SPIF · DSIF · Fracture mechanism

1 Introduction

Incremental sheet forming (ISF) is a flexible, cost-effective, and energy-efficient sheet forming process, particularly suitable for prototype and customized sheet metal products. No special molds/dies or heavy duty forming equipment are required in ISF; thus, it has potentials to overcome the limitations of conventional sheet metal forming processes such as deep drawing and stamping. Leszak [1] first proposed the ISF technology in a US patent in 1967. In the ISF process, the clamped metal sheet is gradually deformed by simple tool(s), which moves along the predesigned toolpaths, as shown in Fig. 1. No special dies are needed in ISF; therefore, time and costs required to design and manufacture dies are largely reduced. Emmens et al. [4] conducted a comprehensive review on the development of the ISF technology and equipment according to the published patents and industrial applications in the past decades. Duflou et al. [5] reviewed wider applications of the ISF process and various ISF process variants. Behera et al. [6] reviewed the SPIF process development published from 2005 to 2015, focusing on the improvement of material formability, process accuracy, and possible ISF applications. Li et al. [7] published a review focusing on the fundamental studies on ISF, including material formability and process modeling. However, the wide-ranging coverage of both review papers omitted the research on material fracture mechanism in ISF as well as in-depth analysis of the material fracture behavior. Various ISF processing strategies were proposed to further improve process capability to prevent material fracture; these included two point incremental forming (TPIF) [8], electricity-assisted ISF adopted by Fan et al. [9] and Van Sy and Thanh Nam [10], and heat-assisted ISF applied by Ambrogio et al. [11], Duflou et al. [12], and Duflou et al. [13]. However, the most widely applied ISF variants are still single point incremental sheet forming (SPIF) and double side incremental sheet forming (DSIF), mainly because of their comparatively simple process setups.

As shown in Fig. 1, only one tool of simple geometry, generally with a small hemispherical head, is used in SPIF. In DSIF, two tools are deployed and positioned opposite to each other on both sides of the metal sheet; thus, the tools can act as movable supporting dies. As a result, the material deformation in ISF accumulates with the movement of the tools. The total time required for the ISF process to produce a part

✉ Hui Long
h.long@sheffield.ac.uk

[1] Department of Mechanical Engineering, The University of Sheffield, Sheffield S1 3JD, UK

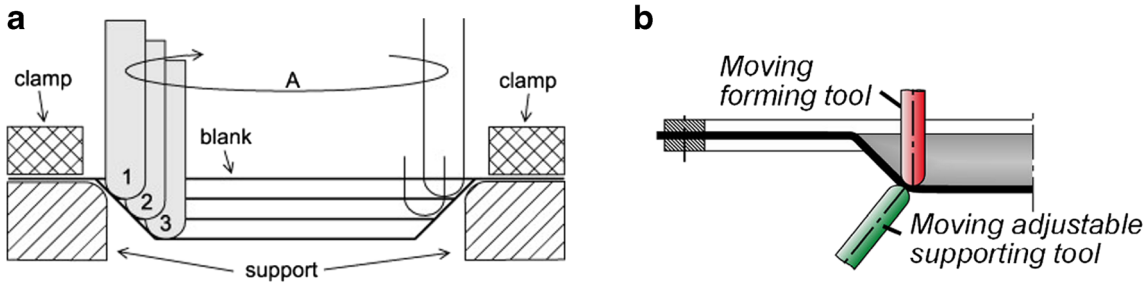

Fig. 1 Schematics of SPIF and DSIF: **a** SPIF for a non-axisymmetric part by Iseki et al. [2] and **b** DSIF with an adjustable supporting tool opposite to the forming tool by Meier et al. [3]

depends on various factors, including the dimensions of the part to be manufactured, the vertical feed of the tool in each circumferential path, and the feed speed of the tool. It usually takes minutes or even hours for ISF to complete one manufactured part, which is quite different from the conventional forming processes. Taking stamping as an example, the overall deformation of the material in the target area finishes instantly in seconds.

According to the experimental tests and finite element (FE) simulations, it has been widely acknowledged that the material plastic deformation in SPIF is limited to the contact area between the tool and the metal sheet. Fang et al. [14] found that plastic deformation also existed in the vicinity of the contact zone by tracing strain evolution of the material elements in and around the contact area. The deformation mode of the material was confirmed to be a combination of stretching, bending, and shearing by conducting investigations through experimental and FE simulations. Jackson and Allwood [15] measured the strain components through the sheet thickness of the ISF-formed parts and identified the existence of stretching, bending, and shearing deformations. Smith et al. [16] confirmed the influence of these deformation modes by comparing stress and strain distributions of the material elements in the thickness direction obtained from FE simulations. Combining the analytical calculations and FE simulation, Maqbool and Bambach [17] obtained the quantitative energy contribution to the plastic deformation from membrane stretching, bending, and shearing effects. Comparing them with the total internal energy, it was confirmed that these three deformation mechanisms dominated in the SPIF process. Incorporating more advanced material yielding criteria into FE simulation which took into account of material anisotropy, Hill's 48 and Yld2004-18 models, Esmaeilpour et al. [18, 19] detected obvious shear strain components in the deformed material elements in the SPIF process. Lu et al. [20] observed the deformed shape evolution of the holes cut through the thickness of ISF parts and found both stretching effect and shearing effect in SPIF. In addition, by conducting the continuous bending under tension (CBT) test, Emmens and Van den Boogaard [21] confirmed that localized material deformation resulted from cyclic effect further extended the forming limit of the materials. Comprehensive literature reviews on the effect of process parameters on the material formability in ISF, including tool dimensions, vertical step down, and sheet thickness, have been reported recently by Gatea et al. [22] and McAnulty et al. [23]. The effect of the compression on further enhancement of the material formability in DSIF was investigated by the experiment conducted by Lu et al. [24] and Moser et al. [25] for accumulative-DSIF (ADSIF).

The research on the material formability in the ISF process can enable the development of an optimized process operation window. By predicting the material processing failure of a forming part in ISF, the optimized process parameters can be selected to enable process or equipment design improvement and to prevent premature material failure of the forming part during the manufacturing process. Furthermore, understanding of the mechanism behind material fracture will help avoid possible defects to be created in the formed part so that the quality and structural integrity of the ISF part can be guaranteed. For a better understanding of material processing failure in ISF, a full analysis of the material response under various loading conditions and how it leads to the material fracture during the process should be conducted.

Fang et al. [14] examined the fracture surface of the failed parts and confirmed that the cracks in the parts manufactured by ISF were ductile fracture. Furthermore, ductile fracture criteria, representing corresponding material deformation characteristics, were applied to predict failure in ISF, which produced satisfactory results compared to the experiments. However, compared with a great amount of research reported on the deformation mechanism of ISF, the study on the initiation and evolution of the material fracture in ISF, especially in DSIF, is very limited. Material fracture mechanisms which occurred in ISF remain unclear. To improve understanding towards the facture mechanism of ISF, a few questions need to be answered.

Firstly, the relative location of the original weak spots and final fracture to the contact area between the tool and the deforming sheet should be ascertained. Different locations of the deforming sheet are subject to different loading conditions and deformation modes. In SPIF, it is obvious that the contact area is subject to contact stress, bending moment, stretching

force along the wall of the forming part, and shear stress along both the tool movement direction and the wall inclination direction. While in the vicinity region around the contact area, the material is mainly subject to the stretching force in the meridional direction. Determining the location of the damage initiation will help to analyze the initiation and development of the material fracture. To identify the location of the initiation of the deformation instability will help to determine the key factors that lead to the instability, which ultimately will lead to the material fracture.

Secondly, to further study the material fracture, the material fracture mechanism in ISF should be investigated. The occurrence of the fracture depends not only on the mechanical properties of the material, but also the stress and strain conditions applied on the material. In terms of ductile fracture, Anderson [26] reported that whether necking was suppressed or not before the fracture occurrence needed to be determined by the stress and strain states. In ISF, two different types of failure modes have been observed, fracture preceded by the necking or abrupt rupture without any obvious sign of necking, reported by Gupta and Jeswiet [27] and by Ai et al. [28] when testing different types of materials. The mechanism behind the transition of two fracture modes is still unclear and needs to be investigated.

This paper presents a review of the enhanced forming limit of materials in ISF, and experimental observations of material fracture. A discussion of the current progress on investigating the fracture mechanism in ISF is provided and future research directions for the ISF process improvement are proposed. Although ISF has shown great potential in manufacturing of non-metallic materials, such as PVC and polymers [29, 30], the scope of this review paper will focus on metallic materials only.

2 Fracture mechanism of SPIF

The research on the material fracture during processing is motivated by defining a safe process operation window. In ISF, the variation of material formability has been observed for a variety of materials deformed when different values of process parameters are selected. Analytical and FE modeling methods have also been adopted to analyze the stress and strain distributions to illustrate fracture initiation in ISF. However, different opinions regarding the location of the fracture and the transition from necking to rupture exist and they are still debated.

2.1 Formability-based studies on material fracture in SPIF

By measuring the strain distribution on the SPIF-manufactured parts of various shapes with material AA1050, Shim and Park [31] reported that the strain state of the deformed material in ISF was between the plane strain condition and biaxial tension condition. More specifically, if the curvature of the ISF-formed part is relatively small, the circumferential contact angle between the tool and the sheet will be small and the strain state will be close to the plane strain condition along the circumferential direction of the part. On the contrary, the strain condition will shift to equi-biaxial tension condition when the curvature of the part is reasonably large. Based on these strain distribution characteristics, conic shapes and pyramid shapes are widely used in the ISF tests as benchmark geometries. For a conic shape, the material is generally assumed to be deformed under the plane strain state, and for a pyramid shape the corners of the geometry undergo the equi-biaxial tensile deformation while the rest of the geometry is assumed to be still under the plane strain condition. Theoretically, a material under biaxial tensile deformation will be under a higher stress triaxiality and greater thickness reduction rate compared with that of the plane strain condition. The stress triaxiality is a widely adopted indicator in assessing the material deformation stability, the greater of stress triaxiality is, the less stable the material deformation is and a smaller sheet thickness leads to higher stresses; therefore, Martins et al. [32] confirmed that the fracture of the ISF-formed pyramid parts commonly appeared at the corners.

Conventional analysis of the ISF process using Forming Limit Curves (FLCs) has been conducted to assess the material formability of the materials in some early studies. Recently, more advanced and detailed analysis of the material deformation in ISF has been reported by using experimental, analytical, and FE methods. These will be reviewed in detail in the following sections.

2.1.1 Enhanced forming limit of materials in SPIF

Materials generally exhibited much higher formability in ISF compared with that in conventional forming processes according to the formability tests conducted using various types of materials, including aluminum alloys used by Shim and Park [31] and Filice et al. [33], copper, steel, and aluminum alloys used by Fratini et al. [34]. In conventional sheet metal forming processes, FLCs or Forming Limit Diagrams (FLDs) proposed by Keeler and Backofen [35] and Goodwin [36] have been widely used to predict the safe operation window for the materials. To plot the FLCs for a tested material, uniform strain values of the specimen upon deformation instability/failure under various loading conditions, such as uniaxial tension, plane strain, and equi-biaxial tension, should be obtained. Banabic [37] reported that the dome test, hydraulic bulge test, and the Nakajima test were widely adopted to obtain

the FLCs for various materials in the industry. The FLCs obtained from the experiments in ISF showed totally different strain limit values and trends upon failure compared with that of the conventional processes. Different from the typical V-shape FLCs obtained from the conventional sheet metal forming processes, formability limit lines with a negative slope in the first quadrant of the major strain and minor strain coordinate system were obtained for various materials in ISF. In addition, the lines were above the FLCs of the conventional processes for each material, especially under the plane strain condition, which showed higher forming limits than that of the conventional sheet forming processes, as shown in Fig. 2.

However, Emmens et al. [38] claimed that FLCs could only be an effective method to predict the formability of the materials under the precondition that plane stress was the main loading condition and a linear strain path was applied. In the conventional forming processes, the critical areas were usually under simple plane stress conditions even though more complicated loading conditions could be present in other areas of the deforming part. Taking deep drawing as an example, the bottom edge of the part was under bending and compression while the wall of the formed part where the fracture generally happened was under simple stretching deformation. While in ISF, however, apart from simple stretching, bending and shearing effects also contributed largely to the material deformation. In addition, progressive toolpaths in ISF created nonlinear loading strain paths. Consequently, as explained by Benedyk et al. [39], the FLCs for ISF could be easily influenced by the process parameters, such as vertical feed and toolpath generation algorithm, which made it unreliable and unrealistic to predict the onset of the fracture accurately for a specific case in ISF. As a result, the FLCs could not be considered as a reliable tool to analyze and predict the processing failure of the materials in ISF. Furthermore, the FLC method was purely empirical; it was not accurate enough to account for the occurrence of fracture in ISF. Further fundamental studies considering the unique deformation characteristics of ISF should be pursued.

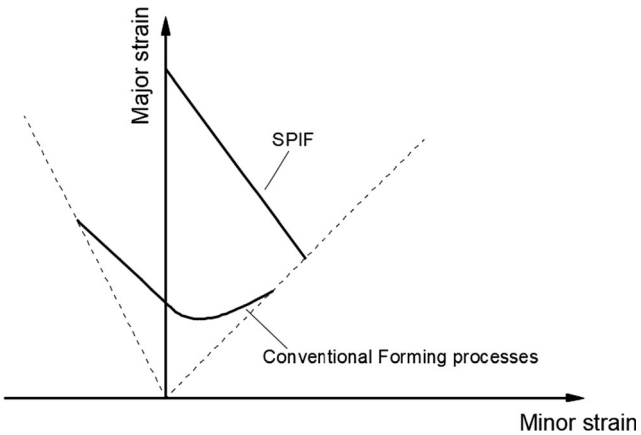

Fig. 2 Comparison of forming limit curves in SPIF and conventional forming processes

2.1.2 Fracture prediction in SPIF

An accurate prediction of the failure could facilitate the design of the SPIF process to avoid premature material fracture of the part to be manufactured. Iseki [40] calculated strain components in the contact area and assumed that the maximum forming depth of the cone part formed by ISF could be predicted once the strains met the strain limit predicted by the empirical Fracture Forming Limit (FFL) under the plane strain condition. To overcome the limitations of the strain-based FLCs for SPIF, Haque and Yoon [41] introduced the stress-based FLCs to predict the formability of the materials. According to their calculations, in the stress-based FLC method, the influence of the loading history was ignored, and a uniform curve was obtained for the process even though different parameters were applied. However, the establishment of the stress-based FLCs for ISF was still based on the strain measurement by the reversed calculation method; direct measurement of the stress components during the manufacturing process was impractical. As a result, although the stress-based FLCs could be integrated into the commercial FE simulation software to predict the occurrence of the processing failure, it still could not provide a fundamental explanation to the fracture mechanism in ISF. Nevertheless, the stress-based FLC method in predicting the material fracture in SPIF was justifiable for the complexity of the ISF process. The combination of the stress and strain states should be taken into consideration in analyzing the fracture initiation in ISF. This is because the effectiveness of the pure strain-induced FLCs in the prediction of the material fracture for conventional forming processes lies in the predictability of the stress state during the process, while in ISF, the contact conditions and the loading paths affect the stress and strain distributions significantly; therefore, it is not feasible to use the strain-based FLC method to predict the material fracture in ISF.

However, in the reported theoretical models to predict the material fracture, it was all assumed that the plastic deformation only occurred in the contact area between the tool and the sheet during the forming process, while only elastic deformation happened in the other areas of the formed part. In addition, the existence of bending was ignored, which will affect the strain/stress distributions substantially, thus making the prediction unreliable.

As mentioned in Section 2.1, FLCs are widely used in conventional forming processes to predict the safe operational window effectively. Similarly, investigations have been conducted to develop a similar prediction tool to predict fracture in SPIF. Based on the FE analysis and experiments using material AA1050-H111, Silva et al. [42] concluded that the failure of the SPIF parts should be predicted by the FFL curves

rather than the conventional FLCs. As can be seen in Fig. 3a, the FFLs for SPIF are quite close to the FFLs derived from conventional fracture tests, especially near the plane strain condition. More similarity between the FFLs from conventional tests and SPIF was reported by Isik et al. [43] by testing the same material AA1050-H111, as shown in Fig. 3b. The same opinion was supported by Martins et al. [32].

Ai et al. [28] compared the thickness of the sheet near the cracks obtained from different tests using materials AA1100 and AA5052-O, including the dome test and SPIF test for different materials under commonly used process parameters. It was found that for one material, a competition between the deformation instability limit and material FFL existed, whoever was reached first, the fracture occurred, as shown in

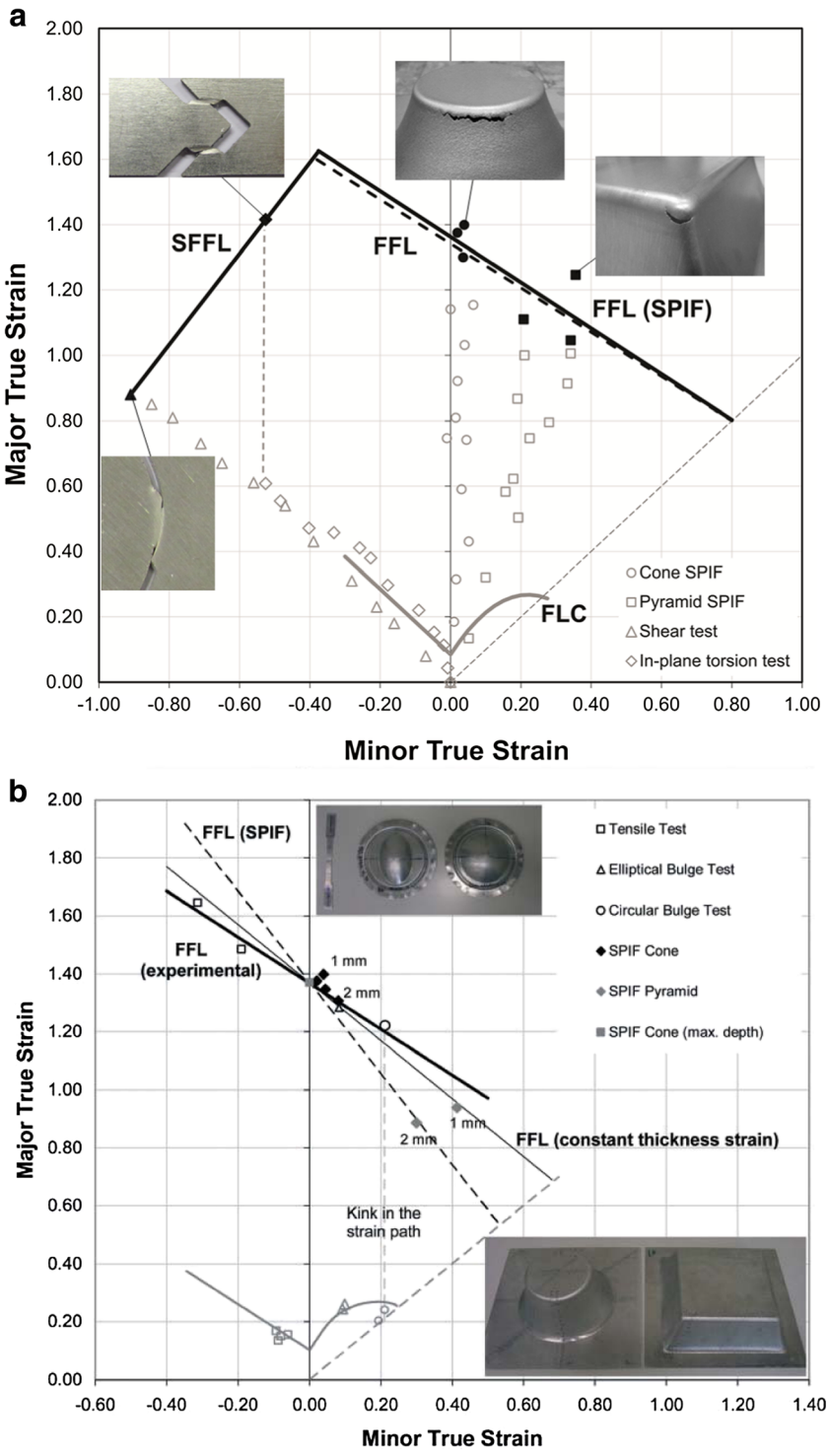

Fig. 3 FLCs and FFLs obtained from material property tests and the ISF tests by: **a** Silva et al. [42] and **b** Isik et al. [39]

Fig. 4. In the first scenario, the onset of the fracture was predicted by the conventional FLCs, while in the second scenario, rupture happened and was predicted by FFLs instead. However, only parameters commonly used in the SPIF were tested during the reported study, even though different fracture behaviors for different materials were captured; the transition from necking to necking suppression may have been overlooked.

By incorporating the FFL curve-related fracture criterion into the FE simulation software LS-DYNA, Suresh and Regalla [44] predicted the maximum forming depth of the conic and pyramid parts with EDD steel. Compared with the experimental results, the maximum error of FEM was below 4%, which was satisfactory. Unfortunately, only one type of material was used; therefore, it was very difficult to justify the advantage of the newly developed model. Nevertheless, the results still supported the conclusion that although the fracture in ISF was delayed, it still could not surpass the intrinsic material fracture point for the material used. Therefore, the fracture forming limit of the material could be a useful solution method for the fracture prediction in SPIF.

2.2 Key factors affecting material formability in SPIF

In SPIF, the sheet thickness distribution of a formed part approximately followed the Sine Law according to the thickness measurement of parts with varied forming angles along the meridional direction by Hussain and Gao [45] and parts with fixed forming angles by Young and Jeswiet [46]. It should be that the larger the forming angle was, the greater the deformation of the sheet could be. Therefore, Hussain et al. proposed that the maximum forming angle could be used as an indicator of the formability of the material in SPIF [47]. Also, although the FLC method was already considered to be not effective in the fracture prediction for the ISF process, it was still a straightforward way to compare the material formability in one set of experiments.

As mentioned in Section 1, the material deformation of SPIF is the result of a combination of stretching, bending, shearing, and cyclic effects, as shown in Fig. 5. A thorough review of the contribution of each deformation mechanism to the enhancement of material formability was reported by Emmens and Van den Boogaard [48]. While a stretching and bending effect was clearly observed in the process, Jackson and Allwood [15] emphasized the existence of through-thickness shear along and perpendicular to the tool movement direction by observing the strain components of the material in the cross-section through the thickness of welded copper plates. Eyckens et al. [49] investigated the effect of through-thickness-shear (TTS) on the material formability under plane strain/equi-biaxial strain conditions by using the extended Marciniak-Kuczynski model. It was found that the existence of TTS could create a slight decrease as well as obvious increase of the forming limit depending on the strain mode. The largest increase occurred when the TTS was in the plane perpendicular to the direction of the major in-plane strain.

The effect of the process parameters on the formability of the material in SPIF is twofold. On the one hand, the process parameters will determine the stress and strain distributions, thus affecting the material formability. On the other hand, a variation of the process parameters brings changes of the relative significance between different deformation modes in SPIF. For example, according to the digital image correlation (DIC) observation by Eyckens et al. [50], the bending effect was more dominant when manufacturing parts with larger wall angle while through-thickness-shear was more dominant for the parts with smaller wall angle. The fracture behavior in ISF could be approximately explained through the perspective of the specific change of geometrical or process parameters. The same conclusion was reported by Maqbool and Bambach [17].

2.2.1 Material mechanical properties

Mechanical properties are the intrinsic properties of a material. They will decide the response of the material to the loading

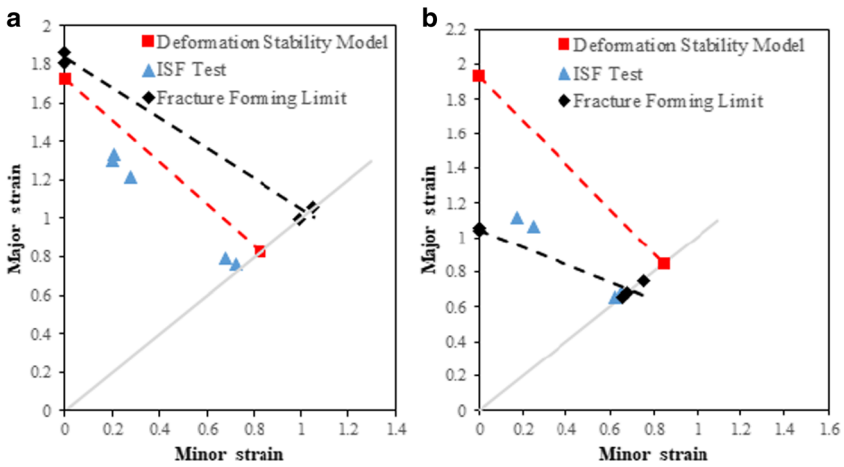

Fig. 4 Comparison between the FFLs obtained from conventional material tests and SPIF tests for: **a** AA1100 and **b** AA5052 [28]

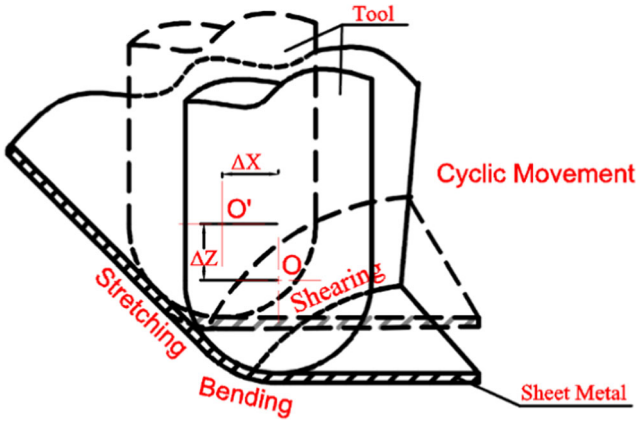

Fig. 5 A schematic of deformation mechanism for SPIF

conditions during the manufacturing process. Various parameters are defined to depict the key mechanical properties of the materials, including hardening coefficient, yielding strength, and tensile strength. Jeswiet et al. [51] manufactured parts of various types of materials with SPIF using the same processing parameters, including aluminum alloys, mild steel, high strength steel, copper, and brass, and found that a huge difference of maximum forming angles existed between different materials. The difference indicated the influence of material mechanical properties on the formability of materials in SPIF. However, how and which mechanical properties affected the formability of the materials in SPIF were not explicitly explored in that work. Ai et al. [28] compared the deformation behavior of materials AA1100 and AA5052-O and concluded that AA5052-O with stronger work-hardening experienced more obvious formability enhancement and neck-to-rupture fracture transition.

To investigate the importance of each mechanical property on the formability of the SPIF process, Fratini et al. [34] conducted a statistical analysis. Various types of materials, including copper, brass, deep drawing quality steel (DDQ), high-strength steel (HSS), and two kinds of aluminum alloys were examined. The homogeneous strains in the meridional and circumferential directions on the outer surface of SPIF-formed parts were measured and FLCs were plotted. By looking into the effect of the mechanical property indicators such as strain coefficient K, strain hardening coefficient n, normal anisotropy index R_n, ultimate tensile strength, and elongation percentage $A\%$ on the FLC, the degree of importance of the properties on the forming limit was identified with the help of the response surface statistical model. K and n were confirmed to be the most important factors affecting the formability of the materials in SPIF. It can be explained by the fact of the incremental nature of the ISF process which made the deformed material tougher due to the work-hardening. Different degrees of work-hardening will determine the material response to the loading.

By employing heat-assisted methods, including laser [12], electricity current [52], hot-air influx [53], or direct heat transfer [54] to raise the temperature in the forming area of the sheet, higher material forming limit and geometric accuracy can be achieved. The reason is obvious because under heat-assisted processing condition, the microstructure of the material can be altered and softened material will yield under lower forming forces, which will postpone the occurrence of the tearing fracture, as explained by Gupta and Jeswiet [27].

The existence of material anisotropy also affected the forming limit of the materials. Kim and Park [55] tested the material AA1050 in SPIF, and it showed distinctive forming limits in the rolling direction and the transverse direction. In addition, the locations of the cracks were influenced by material anisotropy as well. In the experiment conducted, when the tool moved along the rolling direction, the crack appeared under the tool head and it was parallel to the tool movement direction, while when the tool moved along the transverse direction, the crack appeared behind the tool and it was perpendicular to the tool movement direction.

2.2.2 SPIF process parameters

As mentioned in Section 1, varying process parameters in ISF will lead to corresponding change in the forming limit achieved. The most important process parameters in SPIF are tool head size, vertical step size, feed rate, tool rotation speed, and toolpath.

Tool geometry Generally, for the simplicity of the process, tools with hemispherical heads are adopted in ISF. Hussain et al. [56] performed the SPIF process with various tool diameters and reported that the smaller the tool radius was, the higher the material forming limit could be achieved in the process. The enhanced formability was explained by the theory proposed by Emmens and Van den Boogaard [48] that the higher deformation stability could be obtained from localized deformation in and near the smaller contact area. When the tool diameter was too large, the SPIF process degenerated to a conventional deep drawing process and the deformation stability resulting from localized deformation could not be maintained.

However, an adverse trend was observed in the groove test conducted by Kim and Park [55], in which the forming limit of the material AA1050 decreased or stayed the same when the tool size decreased from 10 to 5 mm, as shown in Fig. 6. The difference could be explained by the shape of the tested ISF geometry. Compared with the frequently used geometries, such as conic shapes and the pyramids, the ratio of the size of the tool head to the dimension of the groove was much smaller and the largest stress appeared on the tip of the tool, leading to the fracture. As a result, a totally different fracture behavior was observed.

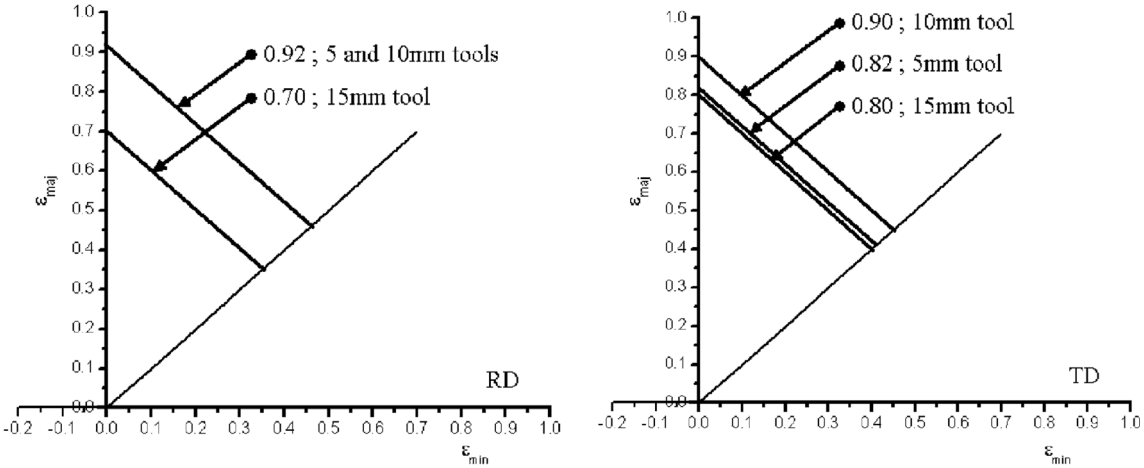

Fig. 6 FLCs for material AA1050 with different tool sizes in the rolling direction (RD) and the transverse direction (TD) [55]

Feed rate The feed rate directly affects the friction conditions between the tool and the sheet. It also affects the strain rate of material deformation. Kim and Park [55] found that when the feed rate was increased from 0.1 to 0.5 mm/s, the forming limit of the aluminum alloy increased in both rolling direction and the transverse direction at the same time, as seen in Fig. 7. However, only one tool size was tested in the experiment and the speed variations tested were limited to a lower range when compared with the feed rate in ISF which could be a thousand times faster; thus, it was the limitation of this study. Hussain et al. [56] tested the forming limit of the material CP Ti at high feed rates from 1200 to 4000 mm/s and found that the forming limit decreased as the feed rate was increased. The relationship between the maximum forming angle of the part and the feed rate could be fitted with a hyperbolic line. The authors attributed the decreased formability to the work-hardening related to the strain rate. However, by comparing the performance of materials, including 304 steel tested by Huang et al. [57], AA5182-O tested by Picu et al. [58], and AA5754 and AA5182 tested by Smerd et al. [59], it can be concluded that different materials showed a varied degree of sensitivity to the strain rate. As a result, the sensitivity of the material to the strain rate could be easily influenced by the feed rate. Kim and Park [55] concluded that aluminum alloy generally showed a lower sensitivity to the strain rate; thus, the formability was less influenced by the feed rate alone.

Tool rotation speed The effect of the tool rotation in SPIF is twofold. The contact between the tool and the sheet will create friction, which can be affected by the tool rotation speed. In addition, friction will generate heat that affects the material microstructure as well as surface topography. As friction also has an impact on the through-thickness-shear, the material formability can be affected. By varying the tool rotation speed, Xu et al. [60] reported that at lower speeds of 0–1000 rpm, friction dominated while when the rotation speed was increased to 2000–7000 rpm, thermal effect took over, as shown in Fig. 8. The enhancement of the material formability at high tool rotation speeds was also observed by Buffa et al. [61] using aluminum alloys and Otsu et al. [62] using magnesium alloys. Durante et al. [63] discovered a drop of friction coefficient at lower rotation speeds from 0 to 600 rpm for material AA7075-T0.

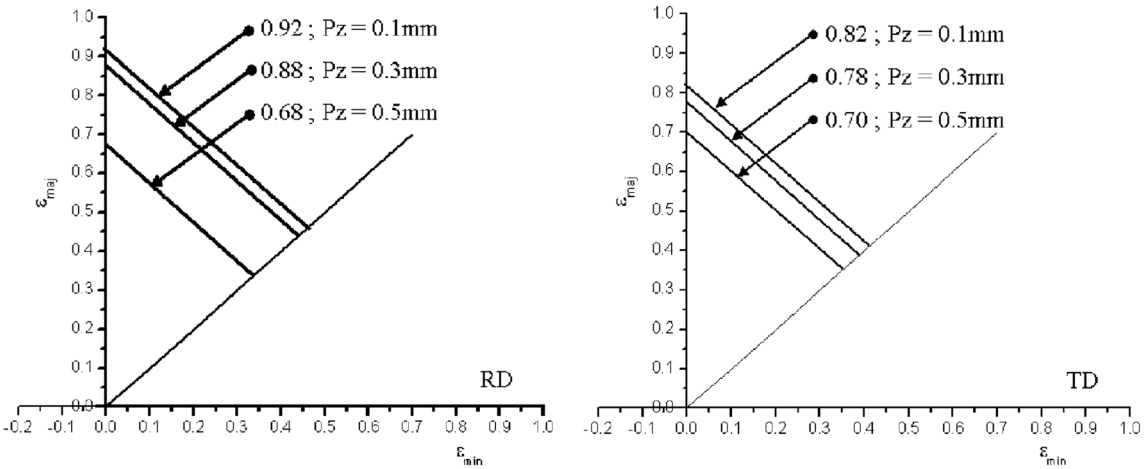

Fig. 7 FLCs for material AA1050 with different feed rates in RD and TD [55]

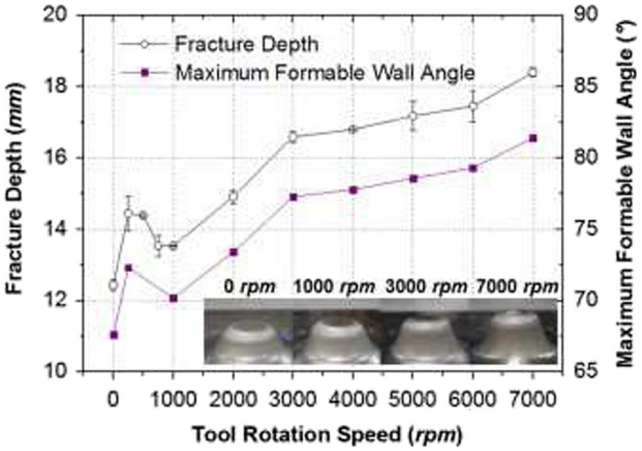

Fig. 8 Fracture depth of parabolic cones at different tool rotation speeds using material AA5052-H32 [60]

Vertical step size Generally, decreasing vertical step size will improve the forming limit of the material because a larger step size will generate a pulling effect due to a large tensile force along the wall of the formed ISF part which will compromise the stabilization effect from the bending in the contact area. The impact of the tool on the sheet resulting from the high-speed movement of the tool will make the pulling effect even more pronounced. The results were reported by Hussain et al. [56] and Micari [64], as shown in Fig. 9a and Fig. 9b, using CP Ti and AA1050, respectively.

2.2.3 Toolpath generation algorithms

Toolpath defines the tool movement contours thus affecting the contact condition between the tool and the sheet, which are crucial to the strain and stress distributions. As a result, both the formability of the material and the geometric accuracy of the ISF-formed part will be affected. The simplest toolpaths are the step-by-step and the helical toolpaths. For the simple geometries, the toolpaths can be calculated mathematically, while for more complicated geometries, Skjødt et al. [65] generated the toolpath directly from the CAD model of the part geometry by the surface milling programs using the conventional CAM software. It was reported how the defining points on the surface were connected to form the contour could affect the formability considerably. Malhotra et al. [66] developed a 3D toolpath generation algorithm for SPIF and found that the developed toolpath algorithm produced the ISF part with higher profile accuracy than the toolpaths generated by the CAM software, as shown in Fig. 10. Lu et al. [67] developed a feature-based toolpath generation algorithm and compared the thickness distribution of the ISF parts with those manufactured using the z-height-based toolpath generation algorithm. It was found that different thickness distributions of the parts were obtained by using different toolpath generation algorithms.

2.3 Deformation-based studies on material fracture in SPIF

The fracture prediction based on the FLCs or FFLs is straightforward and useful for process development and initial analysis. However, it cannot provide an in-depth understanding of fracture initiation and evolution during ISF. In-depth investigations on the fracture behavior have been conducted to analyze damage initiation and evolution in the SPIF process.

2.3.1 Prediction of fracture initiation by analytical modeling

From the perspective of material mechanics, the material deformation behavior and fracture are determined by the strain and stress distributions in the part being deformed. Theoretical prediction of fracture incorporating simple ductile damage models based on the strain or stress analysis was frequently adopted due to its simplicity. By neglecting the force components in the circumferential direction and the friction effect, Huang et al. [68] used the force equilibrium method to derive an approximate estimation of the stress distribution in the contact area between the forming part and ISF tool. Combined with the Oyane damage criterion, the maximum forming angle achievable without fracture in the meridional direction was predicted by solving the following equation:

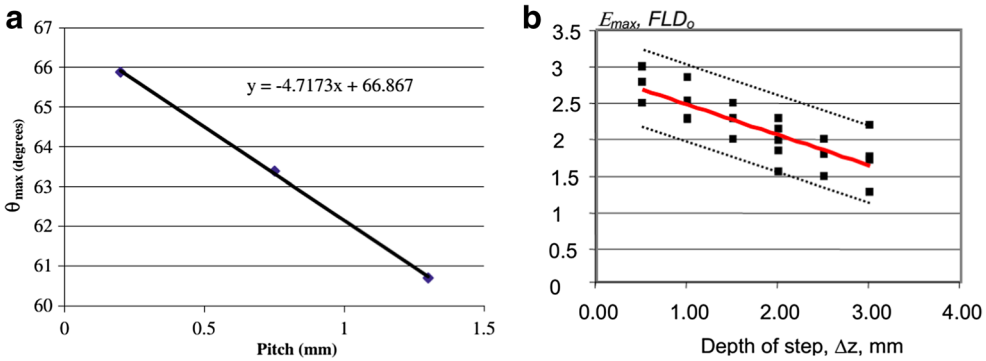

Fig. 9 Material formability related to the vertical step size: **a** maximum forming angle of CP Ti [56] and **b** FLDo for AA1050-0 with a 12-mm-diameter tool [64]

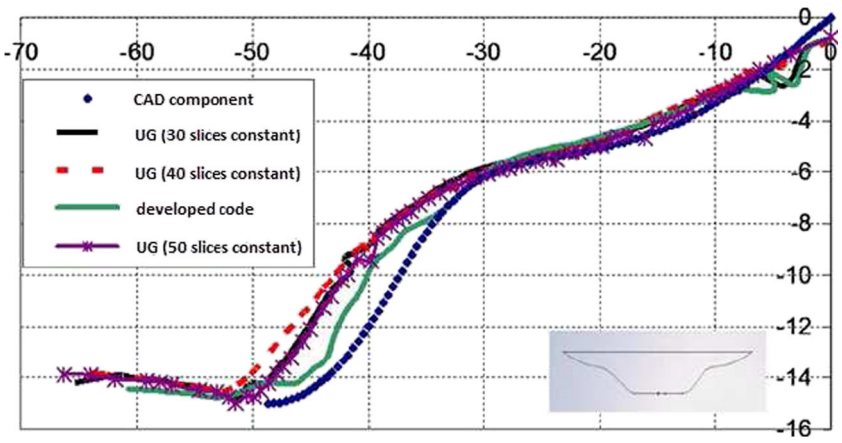

Fig. 10 Comparison of part profiles manufactured by different toolpaths [66]

$$I = \frac{-2}{\sqrt{3}\cdot c_2}\left(c_1 + \frac{\sqrt{3}}{3}\right)\cdot\ln(\cos\phi) + \frac{4}{3c_2}\ln\left(\frac{1+\sqrt{\frac{4}{r_{\text{tool}}^2} - \frac{2\Delta z}{r_{\text{tool}}^3}}\cdot t_0\cdot\cos\phi}{1+\sqrt{\frac{4}{r_{\text{tool}}^2} - \frac{2\Delta z}{r_{\text{tool}}^3}}\cdot t_0}\right)$$

where I is the damage indicator, c_1 and c_2 are constants of the damage model, ϕ is the forming angle, r_{tool} is the tool radius, Δz is the incremental depth, and t_0 is the original sheet thickness. The relationship between the process parameters and the material formability can be easily assessed with the help of the equation. From the equation, it is obvious that the smaller the tool radius and the incremental depth are, the higher the material formability can be, which is consistent with the experimental observations to a certain degree.

Reported theoretical analysis of the ISF process mainly focused on the contact zone where the plastic deformation was assumed to happen due to the localized deformation in ISF. Huang's model [68] assumed a homogenous stress distribution in the contact zone so that the damage variation in that zone could not be reflected in that model. By using membrane analysis, as shown in Fig. 11, Silva et al. [69] calculated the stress distribution in the contact area for the rotational symmetric ISF part. According to their calculations, the tensile stress in the meridional direction can be determined by:

$$\sigma_\varphi = \frac{\sigma_Y}{(1 + t/r_{\text{tool}})}$$

where σ_Y is the yield stress of the material. As a result, the highest tensile stress occurs at the upper boundary of the contact zone where the sheet thickness is the smallest. Furthermore, Silva et al. [69] found that the hydrostatic stress from SPIF was smaller than that in the conventional stamping process, which explained why the forming limit was higher in SPIF.

Their study also concluded that the bending had resulted in an increase of meridional stress. The increase led to a possible localized thinning in the transitional zone between the contact region and the inclined wall of the forming part, as shown in Fig. 12. Combining all these individual effects, the fracture happened at the upper boundary of the contact zone.

On the basis of the membrane analysis, Martins et al. [32] calculated the damage level in the material by adopting simplified fracture criteria considering hydrostatic stress. Based on the calculation, an estimation was made that the strain components in the minor-major space could be fitted into a straight line, similar to the Fracture Forming Limit Diagrams (FFLDs).

In the membrane analysis, the material element for analysis was treated as a shell element and the sheet thickness was ignored; thus, the bending effect was discounted. To make a realistic prediction, Fang et al. [14] calculated stress components taking bending effect into consideration and the equivalent stress across the thickness was determined by:

$$\overline{\sigma}^A = \frac{\sqrt{3}}{2}C_0\left[\ln\frac{t_0(r_{\text{tool}} + t)}{t\left(r_{\text{tool}} + {}^{t}/_{2}\right)}\right]^n$$

where $\overline{\sigma}^A$ is the equivalent stress in the contact zone, C_0 is a constant, t is the thickness of the deformed sheet, and n is the material work-hardening coefficient. According to the equation, the largest stress appears on the outer surface of the upper boundary of the contact zone. Assuming that the vicinity zone also underwent the stress, Fang et al. [14] claimed that fracture started from the outer surface at the vicinity of the contact zone, instead of within the contact zone.

However, the contact conditions in ISF are complex; therefore, the simplified analytical models cannot provide an accurate prediction of the stress and strain states of the material during the ISF process. More details on the deformation behavior in SPIF have been reported, based on FE modeling and their correlations with experiments.

2.3.2 Prediction of fracture initiation by FE damage modeling

FE modeling has been adopted by many researchers to trace material deformation in the ISF process. However, in the common FE models

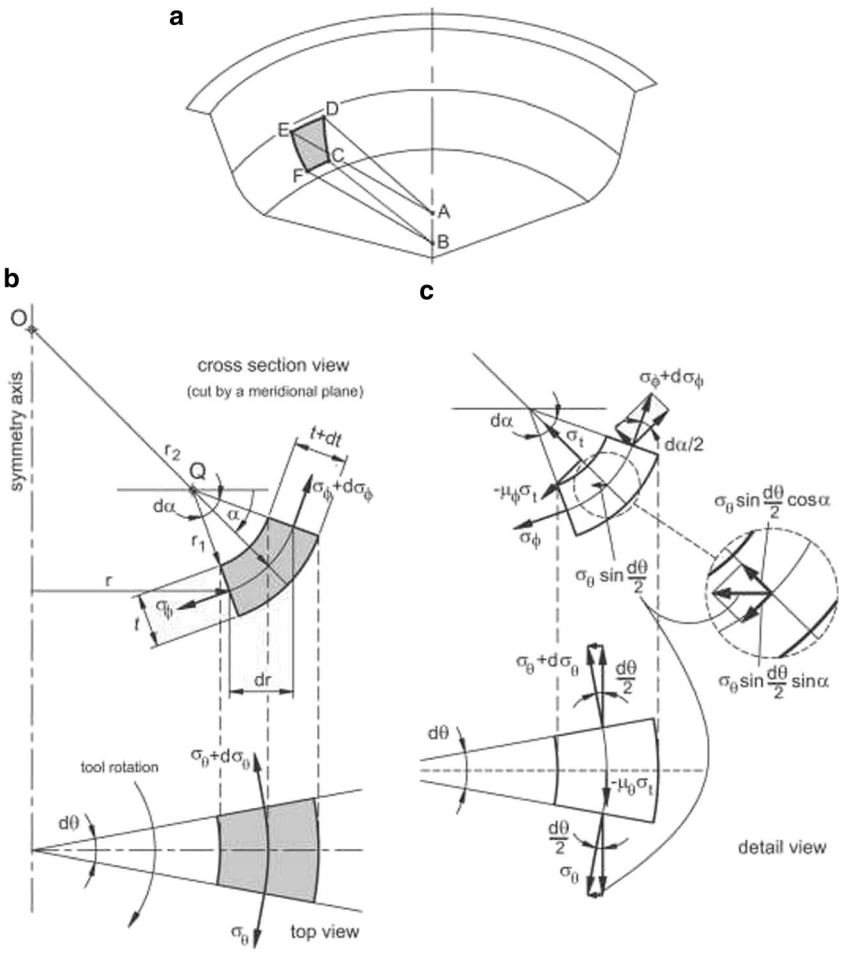

Fig. 11 Schematic representation of the stress analysis by the membrane method for the SPIF process [69]: **a** the extracted element, **b** stress analysis of the element from different views and **c** detailed analysis of the stress decomposition

of the ISF process modeling developed by using the commercial software, the contact conditions and incremental deformation of the material make it difficult to evaluate the damage evolution in the process. To capture the fracture initiation and damage evolution in the ISF process accurately, sophisticated damage models have been incorporated into the commercial FE modeling software.

In order to validate the trend of stress evolution predicted by the analytical model, Fang et al. [14] developed a FE simulation of the SPIF process of a conic shape. The maximum principal strain evolution of an element in the transition area between the formed area and the contact area was plotted in consecutive steps. It was found that plastic deformation not

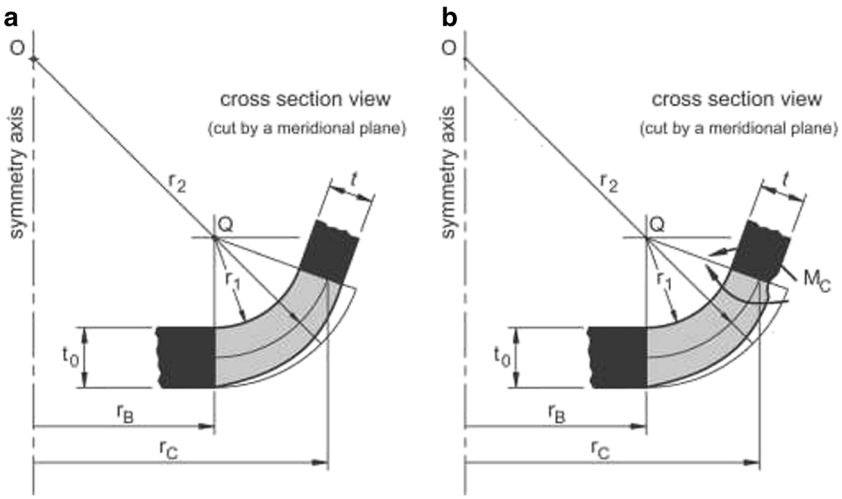

Fig. 12 Possible thinning at the transitional zone [69]: a smooth distribution of thickness without considering bending and b thinning due to the existence of bending

only occurred in the forming zone but also occurred in this transition area, which indicated that fracture could occur in this area, as seen in Fig. 13.

Besson [70] summarized that generally there were two types of ductile fracture models, the micromechanical models and the phenomenological models, depending on the scale used to analyze the initiation and evolution of the fracture. The micromechanical models, such as the Gurson model, were semi-empirical and they were originally derived from rigorous micromechanical analysis, while the phenomenological models, for example the Lemaitre model, were essentially based on the macroscopic considerations.

Various damage models have been used by the researchers in the FE modeling of the ISF process. Unfortunately, different damage models may be only suitable for specific loading conditions. Malhotra et al. [71] introduced a new fracture model into the FE analysis software LS-DYNA to predict the failure in the conic shape and the funnel shape in the SPIF process. By observing the deformation history, it was concluded that it was the cumulative damage resulted from the local bending that led to the ultimate fracture of the parts. Meanwhile, according to the damage variable defined in the developed fracture model, the contact region and the non-contact vicinity region almost had the same level of accumulative damage and hydrostatic pressure. However, there was a huge difference between those indicators on the inside and outside surfaces of the sheet in the same area. Furthermore, the elements on the outside surface of the non-contact vicinity region had a lower degree of through-thickness-shear, which indicated the influence of both bending and shearing on the initiation of damage in SPIF. A similar distribution of the damage accumulation was observed in the simulation performed by Mirnia and Shamsari [72], in which the Modified Mohr-Coulomb (MMC3) ductile fracture criterion was used. Although these simulations provided a good prediction of the possible locations of the fracture in the ISF-formed parts, the relative location between the tool and the crack initiation had yet to be identified.

Wu et al. [74] implemented the modified GTN (Gurson-Tvergaard-Needleman) model in the SPIF process modeling, in which the shear effect was taken into consideration by introducing a shear-affected factor, considering the existence of strong shear strain through thickness direction. Guzmán et al. [73] compared three variants of the GTN damage model to make a better prediction of the damage accumulation in SPIF. However, the results were not in good agreement with the experiments, which essentially acknowledged the complexity of the ISF process and the importance of work-hardening on the fracture behavior in ISF. Nevertheless, the simulation provided an insight into the damage accumulation in ISF; as shown in Fig. 14, the maximum damage occurred in the transition zone between the contact area and formed wall rather than the contact area itself. Gatea et al. [75] also adopted the GTN model with the Nahshon-Hutchinson shear mechanism to predict the fracture when deforming pure titanium. In their simulations, the GTN model with shear mechanism predicted earlier occurrence of fracture; however, more accurate results were predicted in both the conic shape and the pyramid shape than that by the original GTN model, which suggested a clear influence of shear deformation in the SPIF process. In addition, it was concluded that the prediction accuracy of the GTN model was significantly influenced by the mesh density, which explained some of the poor results reported in the literature in which coarse meshes were adopted. Also, a strong effect of tensile stress on the material fracture was reported, as seen in Fig. 15. Yue et al. [76] introduced a fully coupled damage model with material anisotropy and proved the effect of material anisotropy on the damage accumulation in SPIF.

2.3.3 Experimental observations of fracture initiation in SPIF

Simplifications are commonly introduced in developing the analytical and FE models. In addition, the accuracy of the FE modeling of ISF is affected by various modeling considerations, including mesh density, material modeling, and contact condition definitions. The understanding towards the

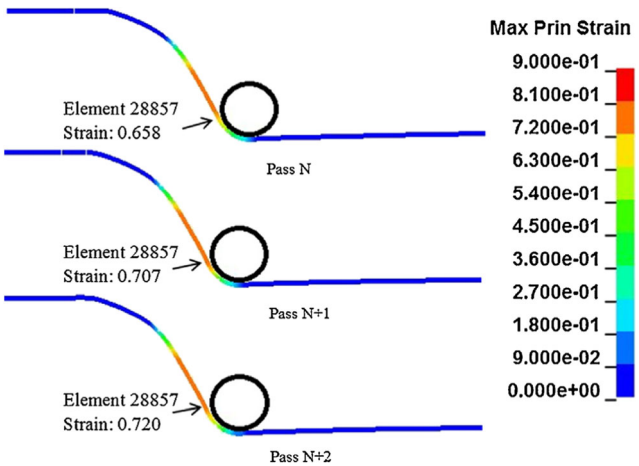

Fig. 13 Maximum principal strain evolution of an element in the cone part under deformation from pass N to pass N + 2 [14]

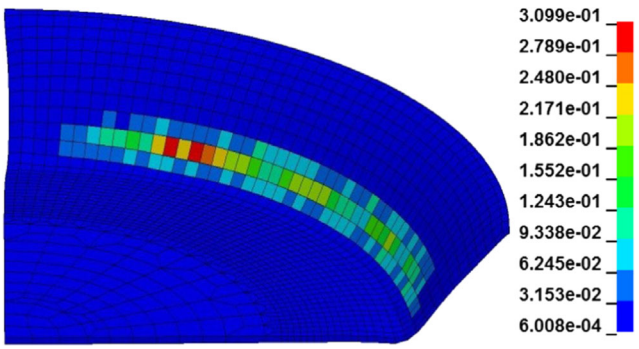

Fig. 14 Porosity distribution for the GTN + Shear + Thomason model when failure occurred [73]

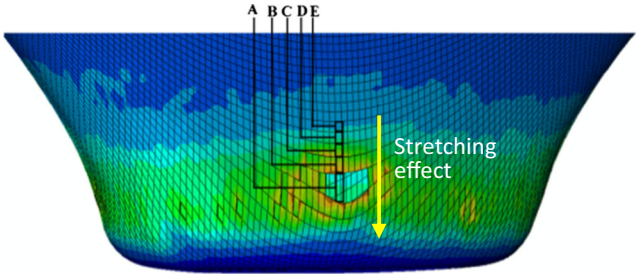

Fig. 15 Numerical results of the porosity for the shear modified GTN model upon fracture [75]

fracture mechanism in ISF can only be better achieved by investigating and analyzing the ISF process experiment itself. Tearing fracture was reported by Fang et al. [14] when manufacturing a conic shape using AA1100, and by Silva et al. [42] when manufacturing conic and pyramid shapes using AA1050-H111. Silva et al. [77] observed a zigzag-shaped fracture in the conic shape and reported that the fracture was triggered by the meridional tensile stress in the plastic deformation zone in the contact area which then propagated to the elastic zone. A similar shape of the cracks was obtained by Hussain et al. [78] and Fang et al. [14]. As can be seen in Fig. 16, it is obvious that the fracture occurred in the vicinity area of the contact zone when manufacturing a conic part with varied wall angles along the depth in SPIF.

The zigzag-shaped crack was a typical appearance of the tension-induced failure under the Mode I loading condition and plane strain condition. Under the plane strain loading condition, the maximum plastic strain occurred at a 45° angle from the crack plane because of the existence of the tensile force; however, the global constrains from the neighboring area created a zigzag pattern according to the ductile crack growth theory, as explained by Anderson [26] in Fig. 17. By tracking the strain evolution history from results obtained from various experiments and numeric simulations, it was

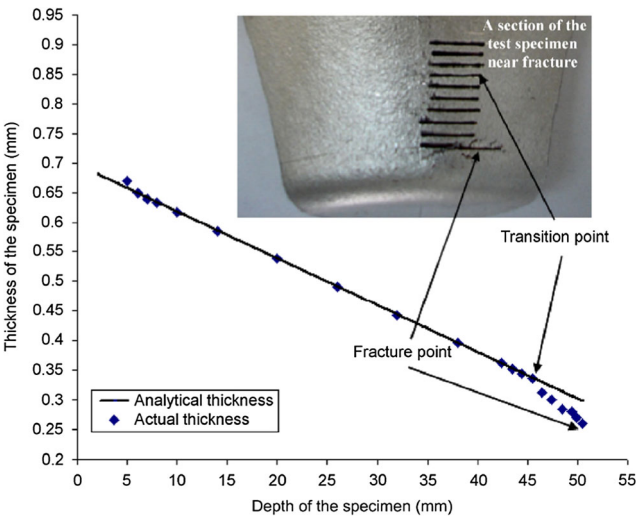

Fig. 16 Schematic representation of a cross-sectional view of the SPIF process [78]

confirmed that in SPIF the strain condition varied from a nearly plane strain condition to a equi-biaxial strain condition when the ratio of the radius of the forming tool to the curvature of the part was increased. For the conic shape, the ratio of the radius of the forming tool to the curvature of the part is quite small; the material would be under a plane strain condition generally.

However, without further experimental evidence, it is very hard to confirm the exact location of the fracture initiation. Different from the observation by Silva et al. [77], Fang et al. [14] observed the fracture initiation in a conic part by using a high-speed camera and found that the first fracture occurred just in the transition zone between the contact area and formed wall. Dwivedi et al. [79] manufactured a truncated cone with a large forming angle until fracture happened using material AA1050-H14. As shown in Fig. 18, the crack was slightly above the contact area.

A "transition point" was also found where the thickness of the sheet started to be obviously reduced than the predicted thickness distribution in both the experiments using aluminum alloy and CP Ti, as shown in the parts manufactured by Hussain and Gao [45] in Fig. 19 and by Hussain et al. [56] in Fig. 20. It indicated that the fracture of the material in SPIF was an intrinsic property of the material. In addition, Hussain et al. [56] observed numerous microcracks above the visible crack and attributed it to the necking-like phenomenon in tensile tests. By comparison, multiple visible neckings were observed by Malhotra et al. [71], as shown in Fig. 21.

In order to explain the suppression of the necking phenomenon, a *Noodle Theory* was proposed by Malhotra et al. [71]. According to this theory, although the bending compromised the damage accumulation reduction resulting from the shearing effect, the weaknesses created in the previous passes took a share of the total necking so that the final necking was postponed. An illustration of the proposed theory is shown in Fig. 22. Therefore, instead of obeying the necking theory, developing a new damage model may be required as a more appropriate method for predicting the fracture of the ISF process.

2.3.4 Suppression of necking in SPIF

In the ductile fracture, it was common that localized necking appeared before the final fracture happened for the processes in which stretching was the leading deformation mechanism, as reported by El-Sebaie and Mellor [80]. Silva et al. [81] and Madeira et al. [82] observed a necking phenomenon in the parts produced in SPIF by using conventional deep drawing steel and AA1050-H111, respectively. Bambach et al. [83] detected visually noticeable necking when using the material DC04 with a sheet thickness of 1.0 mm in an incremental groove test, as shown in Fig. 23. The necking of the sheet appeared in the contact area near the lowest point of the tool.

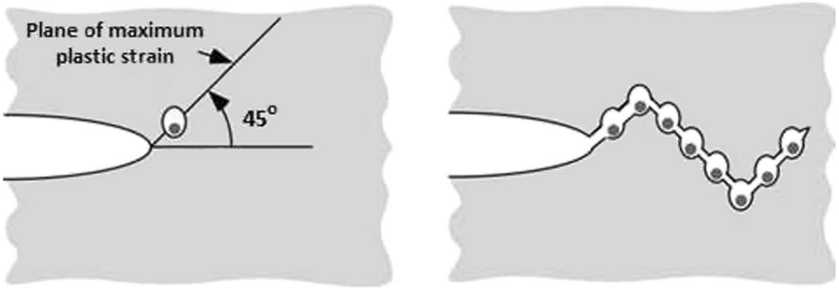

Fig. 17 Development of the zigzag pattern crack [26]

However, the width of the groove was almost equal to the diameter of the tool; the features of ISF deformation were not fully represented by the groove test. The relative dimension of the tool to the part was far too large compared to that in the actual ISF experiment, thus creating a distinctive contact conditions therefore a different stress/strain distribution. Furthermore, it was found that the Fracture Forming Limit (FFL) for SPIF varied with different testing geometries, process parameters, and strain paths, which contradicted the conclusion made by Silva et al. [81]. This indicates that the fracture behavior in SPIF should not be an inherent property of the material only; it should also be process-related. The fracture mechanism in ISF is far more complicated than that in the conventional sheet metal forming processes due to the existence of the multiple deformation mechanisms and complicated toolpaths.

However, in the experiment conducted by Silva et al. [42] with the material AA1050-H111, no previous necking was observed before the final fracture, which indicated once the thickness strain had reached a threshold value, abrupt fracture from uniform thickness occurred without any sign of necking. This shows that the fracture of the part purely depends on an inherit property of the material; thus, a fracture forming limit line (FFL), instead of the traditional V-shape curve, should be used to predict the forming limit of the material in SPIF.

An interesting theory was proposed by Emmens and van den Boogaard [84] that the necking zone in the contact area lost contact with the tool, as shown in Fig. 24, thus minimizing the effect of stress concentration on the development of the necking based on the yield criterion. Based on this explanation, the forming limit of the material could be enhanced.

Because stretching and bending were two of the main deformation mechanism in SPIF, for the purpose of comparison, Nakazima tests were conducted by Centeno et al. [85] to obtain the FLC of the material AISI 304 steel sheet with a thickness of 0.8 mm, as shown in Fig. 25. In the tests, a cylindrical punch was used to push the specimens to certain depth until fracture took place therefore the fracture behavior of the specimen under stretching and bending condition could be investigated. No prior necking was observed before fracture by the eyes or even DIC devices during the tests. However, by observing the thickness distribution of the specimen near the cracks, necking was confirmed to appear in a considerably short time before the fracture happened. As a result, the authors proposed that the failure mode in ISF was postponed necking followed by ductile fracture. However, the clear evidence of the necking phenomenon depended on the degree of bending deformation, which was controlled by the ratio of sheet thickness to the tool radius t/R_0. It was concluded that the bending effect was not the only factor that improved the formability of the material, evidenced by the difference between the forming limits of the material under ISF and stretch-bending tests. This study provided a valuable insight into the fracture behavior in ISF.

Both failure phenomena were also observed by Silva et al. [81] in the same setting of experiment by changing the tool size. As shown in Fig. 26, when the incremental tool ratio (the

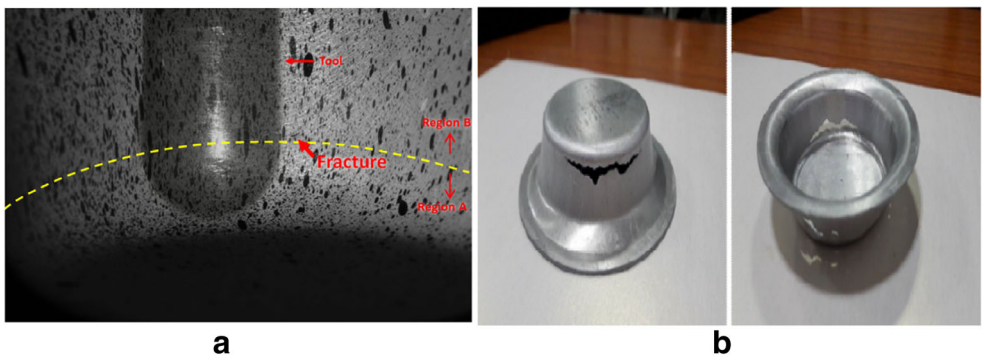

Fig. 18 Fracture not in the contact zone: **a** fracture location [14] and **b** fractured truncated cone part [79]

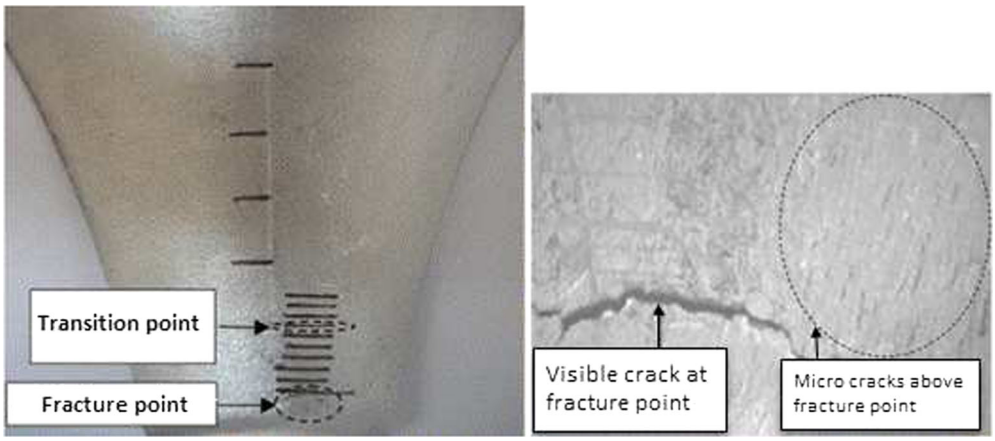

Fig. 19 Section view of the fracture part made using aluminum alloy by Hussain and Gao [45]

ratio of the part radius to the tool radius) was increased, the failure behavior for material AA1050-H111 changed from abrupt rupture to necking. The transition of the failure modes was explained by the stabilizing effect from the dynamic tension under bending. When the tool radius was large, the stabilizing effect was not strong enough to suppress the necking phenomenon compared to the tools with smaller sizes. However, there was only one material being investigated in this study which also revealed that different materials presented different fracture behaviors even under the same experimental conditions. The influence of the material mechanical properties should also be taken into consideration.

In the experiment conducted by Ai et al. [28], two types of materials, aluminum alloys AA1100 and AA5052-O, were tested using the same sets of process parameters. In addition to bending, the influence of material properties on the deformation and fracture behaviors was investigated. The conic shape and the pyramid shape with an increasing wall angle were adopted, representing plain strain and equi-biaxial tension conditions. Fracture occurred when the depth of the part reached a certain value. The thickness distribution along the meridional direction near the cracks in ISF parts were compared with that under the bulge test, which is a widely used method to predict the forming limit of the materials in the conventional sheet metal forming processes. As shown in Figs. 27 and 28, obvious necking can be found in the AA1100 sheet under deformation conditions in both ISF and bulge tests. However, for the AA5052 sheet, necking appeared before the fracture in the bulge test while only abrupt fracture could be observed

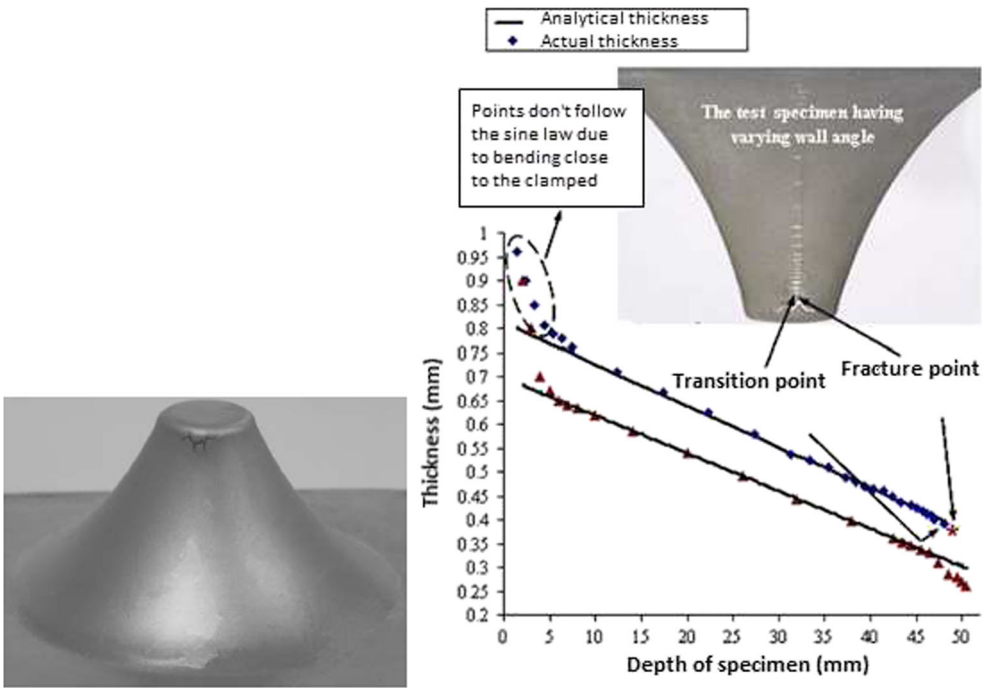

Fig. 20 Section view of the fracture part made using CP Ti by Hussain et al. [56]

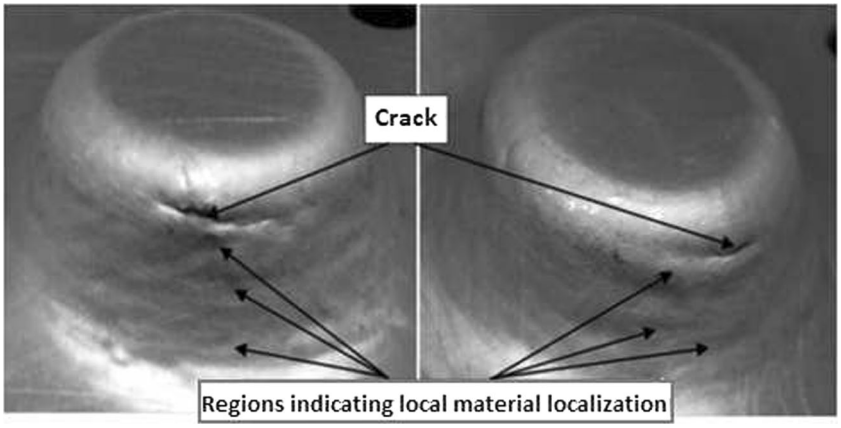

Fig. 21 Multiple necks observed from the outer surface of truncated cones [71]

during the ISF process under both plain strain and equi-biaxial tension conditions, indicating that necking was suppressed in the AA5052 sheet in SPIF.

The transition from fracture-initiated failure to necking-initiated failure while the tool radius was increased was attributed to the bending effect, according to the investigations conducted by Centeno et al. [85]. This is because when the bending effect was moderate, the through-thickness strain/stress gradient was limited; the final fracture of the sheet depended on the total deformation instability of the sheet across its thickness. Therefore, the fracture of the part was determined by the plastic instability of the inner side of the sheet due to its relatively lower tensile stress resulted from the compression effect produced by bending, and necking happened eventually. While when the bending effect was severe, the through-thickness strain/stress gradient was increased, a crack occurred even before the whole sheet across the thickness entered the zone of deformation instability. As a result, the fracture of the part was determined by the plastic instability of the outer side of the sheet. Once a crack initiated on the outer surface, it propagated instantly and fracture happened without the development of necking. Morales et al. [86] suggested a similar opinion and proposed a mathematical model to further explain this phenomenon. In the proposed model, fracture took place when the maximum values of tensile force, ν and bending moment, μ, were reached. Depending on the ratio of the force to the moment, limit lines indicating the onset of different types of failures were plotted, as shown in Fig. 29. Necking-controlled fracture happened when the strain in the concave side of the sheet reached a certain value (curve a-b). When the strain in the concave side of the sheet reached a certain value (curve d-c), fracture-initiated failure took place. With the increasing of the ratio, the fracture mode transited from fracture-initiated failure to necking-initiated failure, which was consistent with the experiment conducted by Silva et al. [81].

An explanation to the transition of the necking phenomena was given by Stoughton and Yoon [87]. In their theory, as

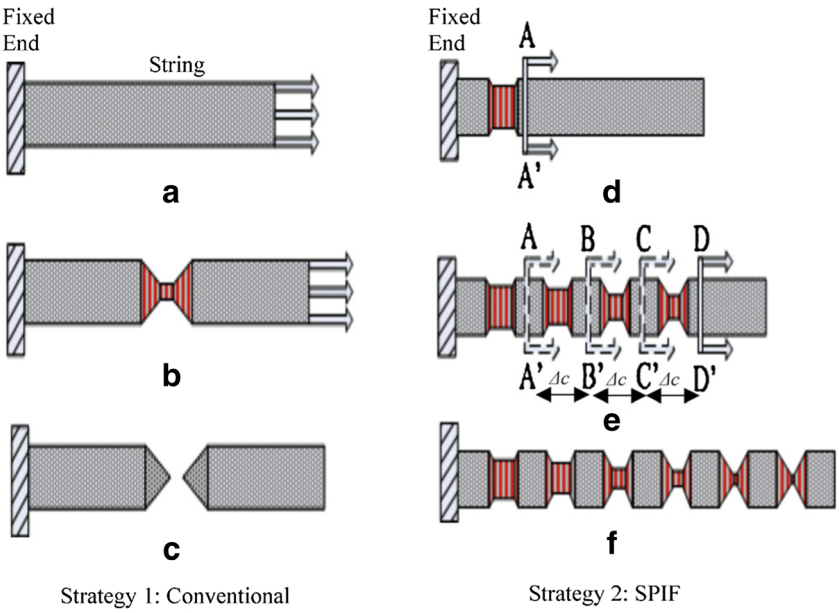

Fig. 22 Schematic of the Noodle Theory proposed by Malhotra et al. [71]

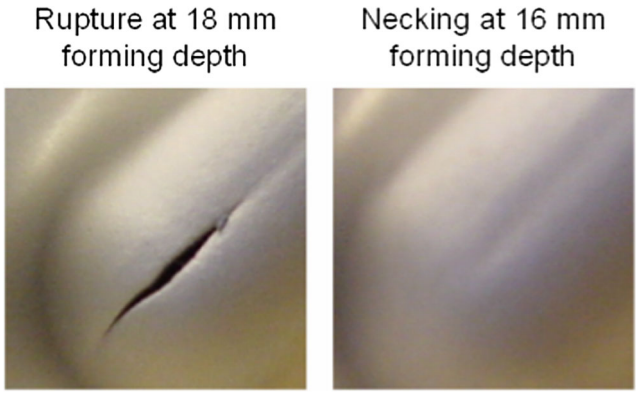

Fig. 23 Fracture and precedent necking in the incremental groove test using DC04 [83]

shown in Fig. 30, only when the compressive stress resulting from the bending of the tool on the concave side of the sheet was overcome by the superimposed high tension, and the whole section of the sheet was under tension, necking became possible. A similar theory was proposed by Seong et al. [88], in which the occurrence of necking of the material under bending preceding the fracture depended on the magnitude of the superimposed tensile stress. If the tensile stress was large enough, necking happened first.

2.4 Material testing methods representing the deformation mode in SPIF

Apart from the direct approaches on testing the ISF process itself, various studies were conducted to replicate the deformation modes in ISF by developing novel material testing methods. The most appropriate representation is the continuous bending under tension (CBT) test. The CBT test was first proposed by Benedyk et al. [39] to investigate the enhanced formability of materials and then explored by Emmens and Boogaard [21] for SPIF. In the CBT test, as shown in Fig. 31,

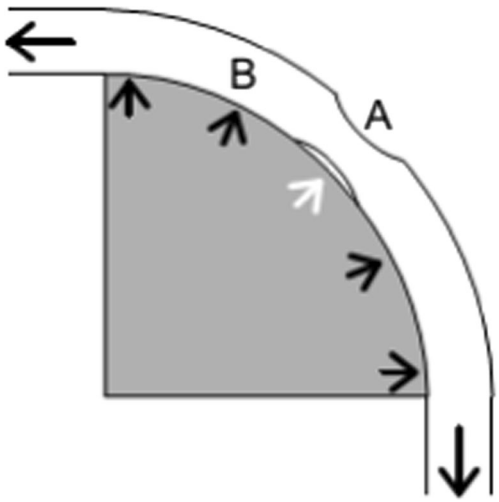

Fig. 24 The neck loses contact with the tool [84]

the complicated contact conditions in ISF are simplified into a two-dimensional model. The stretching, bending, and cyclic effects are superimposed onto each other. They can be independently investigated by simply changing the controlling parameters of each deformation. For example, the bending depth of the roller could change the degree of bending, while the traveling speed of the rollers could vary the frequency of the localized deformation. Using CBT tests, localized deformation and lower levels of tensile force were observed. In addition, multiple necks were observed on failed specimens, which could be supportive to the *Noodle Theory* proposed by Malhotra et al. [71]. It was also observed that when the stretching speed was high enough, the CBT condition was degenerated to be simple stretching and the bending effect was less noticeable. Hadoush et al. [89] performed complementary finite element simulation of the CBT test and tracked the tensile stress distribution across the thickness of the specimen. It was found that the fracture of the CBT specimen occurred when the bending effect was overcome by the tensile effect and the whole thickness section was under tensile stress. A similar test was performed by Barret et al. [90] using material AA6022-T4.

3 Fracture mechanism of DSIF

In spite of its high process flexibility, SPIF has limited applications in the industry due to the relatively low forming accuracy of the manufactured parts. Micari et al. [91] suggested that lower forming accuracy in ISF mainly results from three factors: springback, pillow effect, and excessive bending around the inner boundary of the backing plate. Several ISF process variants were proposed. TPIF reduced the springback by providing supporting force on the other side of the sheet using a half die, which reduced the stress gradient resulting from the bending effect across the thickness and the tensile force along the depth direction, while electricity-assisted ISF and other heat-assisted ISF improved the forming accuracy by reducing the forming force due to the softening of the material during the manufacturing process. However, the flexibility and cost of the ISF process are compromised in these alternative ISF methods due to the introduction of the auxiliary equipment in manufacturing.

Double side incremental sheet forming (DSIF) improves the forming accuracy without sacrificing the flexibility of the process by introducing a supporting tool as a partial die on the other side of the sheet metal. Instead of using one forming tool as that in SPIF, two independently controlled tools are deployed in DSIF, one on each side of the sheet. The relative position of the two tools can be adjusted. When the supporting tool is pressed against the forming tool, additional compressive force is applied, as shown in Fig. 1b. As a result, the gradient of the stress in the radial direction is reduced, so is

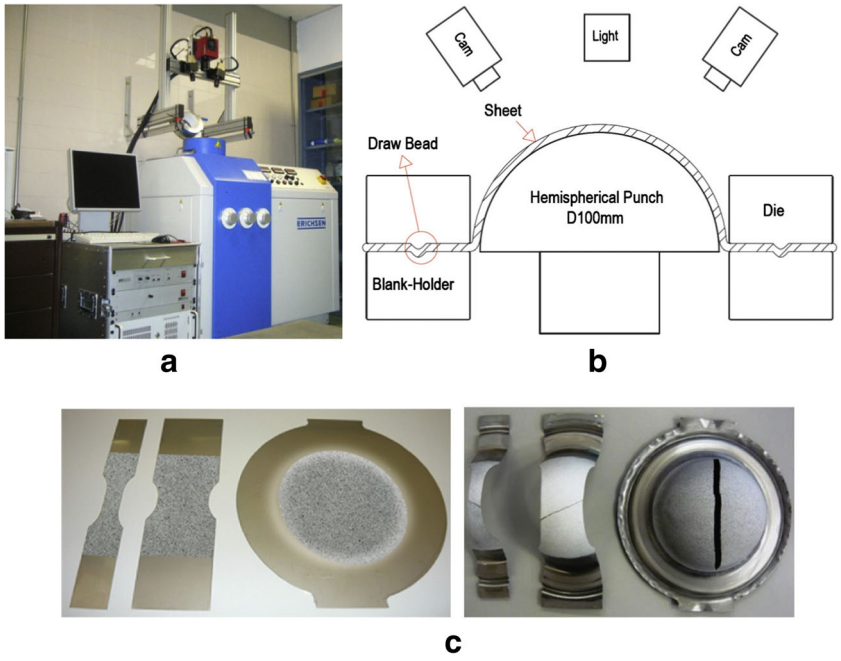

Fig. 25 Nakazima tests equipment and specimens before and after the tests [85]: **a** test equipment, **b** schematic of the test configuration and **c** specimens before and after the tests

the tensile stress in the inclined wall direction. In addition to increasing the forming accuracy of the part, Malhotra et al. [92] compared the forming depth of conic shapes manufactured by SPIF and DSIF and reported that the forming limit of the material was further enhanced in DSIF. Furthermore, with the reduced tensile force, no backing plate of a specified shape is needed to assure the geometry of the edge of the part; thus, the manufacturing cost and time are further reduced. As a result, in addition to maintaining all the advantages of SPIF, DSIF has improved forming accuracy with greater material formability as well as enhanced process flexibility when manufacturing highly complicated geometries using the designed DSIF equipment or platform, as shown in the parts made by Wang et al. [93] and Smith et al. [16].

DSIF, however, requires a relative complex tool system compared with SPIF. Based on the traditional CNC machine, a C-shaped frame was designed by Wang et al. [93] at Northwestern Polytechnic University as shown in Fig. 32a. By changing the slots of the supporting tool, the relative location between the two tools could be adjusted. However, because of its simple and effective tool adjustment mechanism, it lacked structural stiffness and operational accuracy. To improve the tool movement of the DSIF process, purposely built experimental platforms were developed

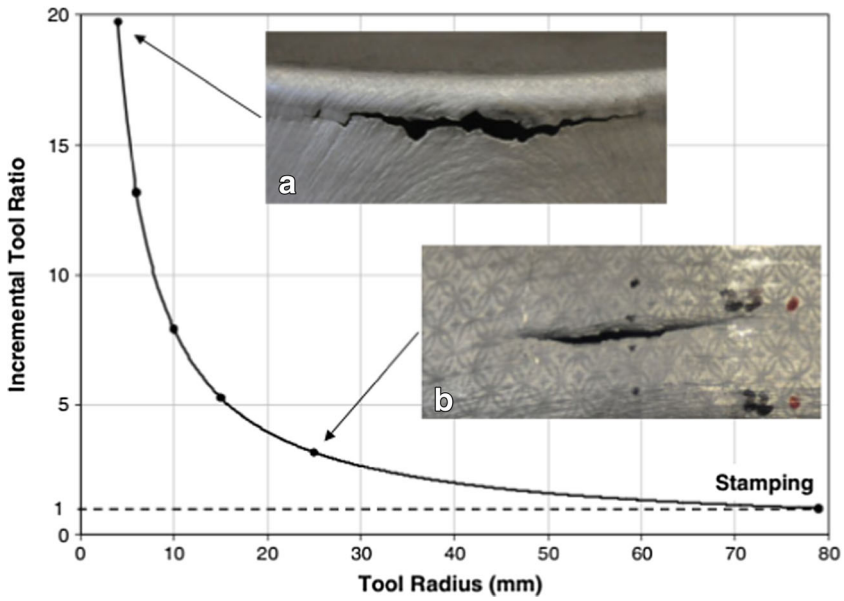

Fig. 26 Two different kinds of failure in ISF with different incremental tool ratios and tool radiuses: **a** fracture with suppression of necking and **b** fracture with necking [81]

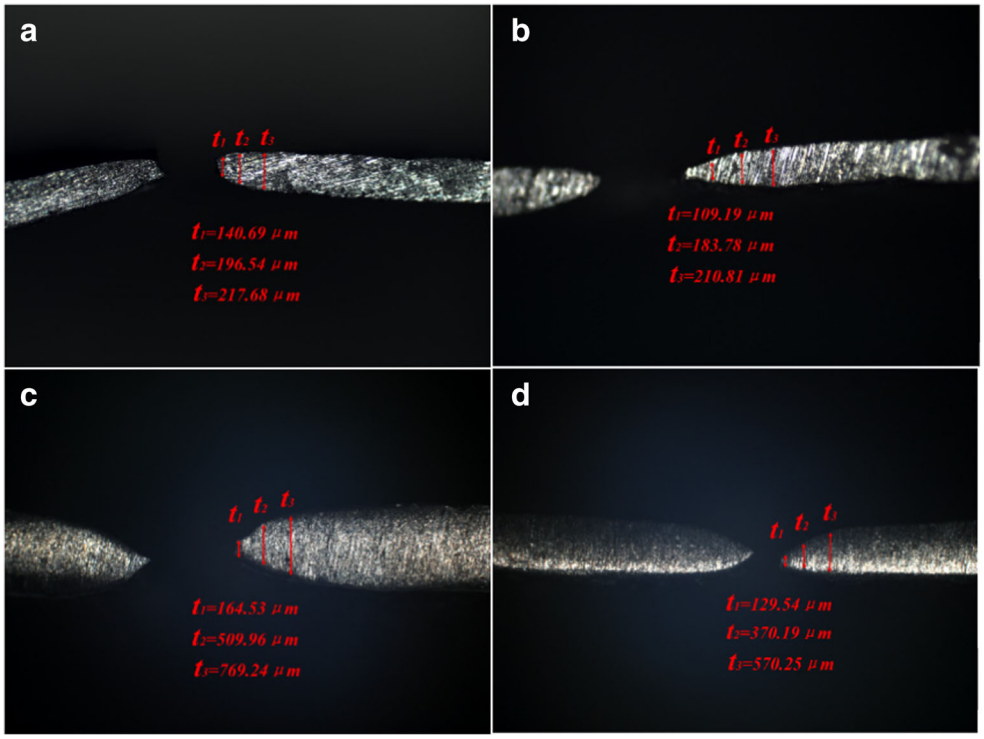

Fig. 27 Cross-sectional view of the fracture region for the AA1100 material: **a** cone part in the ISF test, **b** pyramid part in ISF test, **c** bulge test part under plane strain condition, and **d** bulge test part under equi-biaxial stretching condition [28]

in Northwestern University by Malhotra et al. [94] and Shanghai Jiaotong University by Lu et al. [24]. In both platforms, both tools could be independently controlled, giving more flexibility of tool movements, required by the DSIF process. Different from the traditional CNC machine-based DSIF platforms, industrial robots were utilized to perform the DSIF process. Owing to the high control precision of the robots, the relative position of the two tools, represented by the angle between the line connecting the centers of the tools and the perpendicular line, could be easily changed. Meier et al. [95] deployed two inter-connected industrial robots to move simultaneously along the defined toolpath in the DSIF experiment, as shown in Fig. 32c.

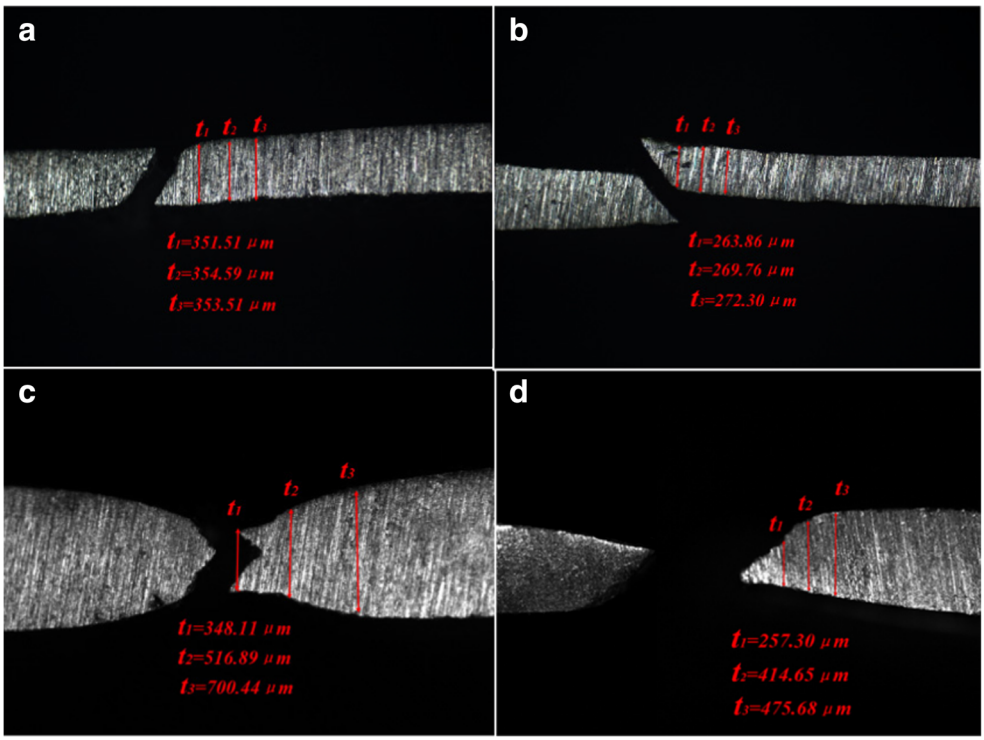

Fig. 28 Cross-sectional view of the fracture along the meridional direction for the AA5052 material: **a** cone part, **b** pyramid part in the ISF test, **c** bulge test part under plane strain condition, and **d** bulge test part under equi-biaxial stretching condition [28]

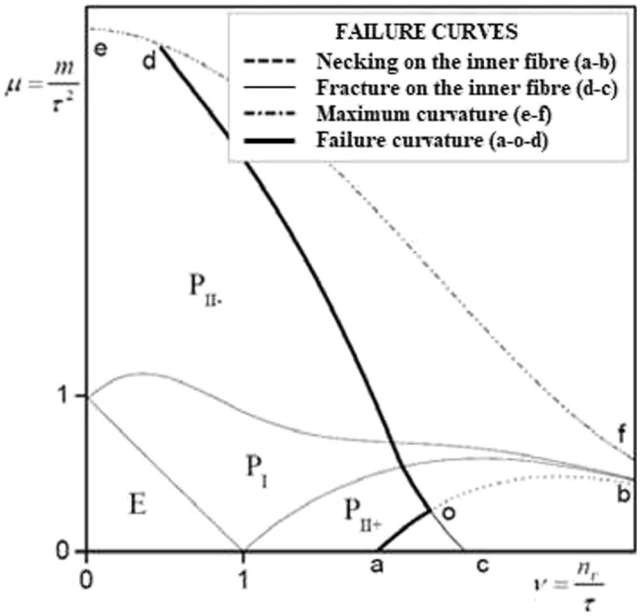

Fig. 29 M-N diagram with relation to the failure mode in stretching under bending [86]

In most cases of the ISF processing, including SPIF and DSIF, the tool(s) starts from the outer boundary of the geometry and moves inwards to the center of the deforming sheet. On the contrary, Malhotra et al. [94] developed another toolpath generation method called accumulative-DSIF (ADSIF) in which the tools moved outwards to the edge from the center. Compared with the inwards toolpath DSIF, the tensile force produced by ADSIF onto the formed part was much smaller; thus, less springback occurred after the whole part was manufactured and better forming accuracy of the parts was obtained with the same process parameters. However, Xu et al. [96] reported that the vertical step adopted in ADSIF had to be smaller than a certain value (0.025 mm) to guarantee the forming accuracy, making the manufacturing time longer than the DSIF using the inwards toolpath.

The introduction of a second tool on the other side of the sheet brings more complexity to the contact conditions in the DSIF process. According to the contact between the tools and the sheet, in DSIF, the part can be divided into four regions, dual-contact region, two single-contact regions, and non-contact region. In terms of the deformation mechanism, apart from stretching, bending, and cyclic deformation, additional compression (squeezing effect) is also introduced into DSIF.

An obvious drawback of the current developed DSIF platforms, including the robot-assisted DSIF, is the loss of contact of the supporting tool with the sheet during the deformation, as observed by Malhotra et al. [92], Meier et al. [95], and Xu et al. [96] in their platforms, respectively. Generally, the movement of the tools is determined by the coordinates predefined by the toolpath generation algorithms. It will result in less accurate thickness distribution of the sheet in DISF if the supporting tool is not placed in the ideal position, or excessive thinning of the sheet or the deflection of the structures occurs if the supporting tool will lose its contact with the sheet; therefore, DSIF degenerates to SPIF. Because a material generally shows a lower formability in SPIF, therefore, the loss of contact leads to a premature failure in the DSIF process. The loss of contact can be effectively prevented by using the ADSIF strategy or using a non-fixed tool supporting mechanism. For example, the tool may be mounted on a compressed air cylinder in the machine developed by Lu et al. [24], so the pressure provided by the compressed air cylinder will push the tool against the deforming sheet to maintain the contact with the sheet all the time. Although the relative location between the two tools could shift from the designed position due to the push from the supporting air, the contact zones will change accordingly, while A force sensor was adopted by

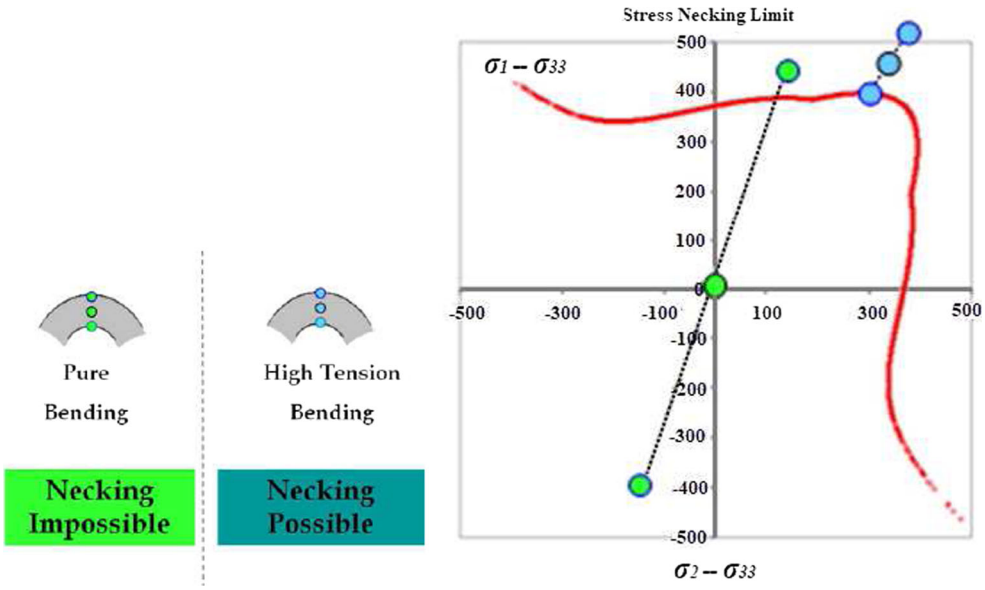

Fig. 30 Failure modes in pure bending and stretch-bending according to the stress necking limit diagram [87]

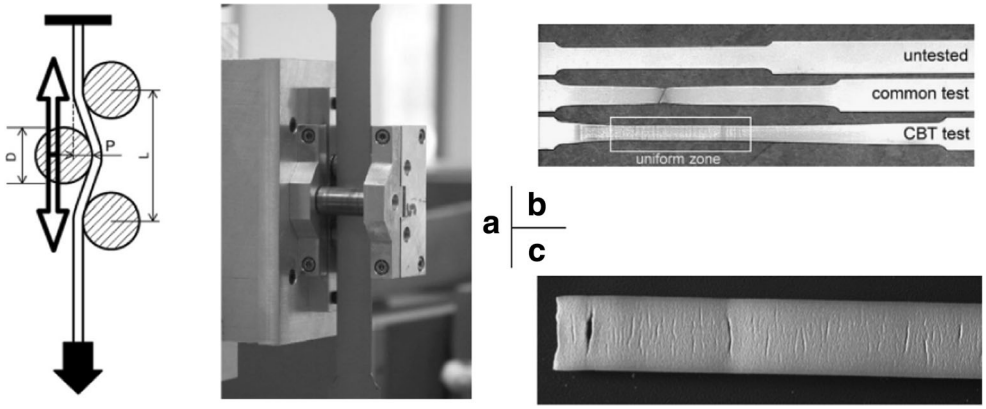

Fig. 31 The CBT test performed by Emmens and Van den Boogaard [21]: **a** the schematic and key mechanical component of the CBT test, **b** the comparison between the tested specimens, and **c** diffuse multiple necks in a specimen

Meier et al. [3] on the supporting tool so that the contact condition of the supporting tool was monitored, and the displacement of the tool was corrected once a loss of contact was detected.

To simplify the analysis of the process, DSIF was generally treated as SPIF with a superimposed supporting compressive force. A general account of the effect of the compression force on the formability of the DSIF process was discussed by proposing a theoretical method by Lu et al. [24]. In the FE modeling investigations, most of the current studies only focused on the dual-contact region [16]. However, compared with SPIF, experiments and FE simulations performed to explain the initiation and evolution of the fracture in DSIF are very limited, probably due to greater difficulties in performing DSIF than SPIF.

3.1 Key factors affecting material formability in DSIF

In addition to the process parameters affecting the deformation behavior in SPIF as outlined in Section 2.2.2, which includes material mechanical properties, vertical step size, tool size, and feed rate, for DSIF, the relative position of the tools and the magnitude of the compressive force exerted by the supporting tool also affect the forming limit of the materials substantially. Meier et al. [3] changed the supporting force and the relative position of the tools and achieved a maximum increase of the drawing angle by 12.5% with optimized parameters of 300 N and 30 degree using alloy AlMn 99.8 1hh, as shown in Fig. 33.

3.1.1 Compression from the supporting tool

In general, the existence of the imposed compressive force increased the formability of the materials, as reported by Smith et al. [97]. The tool compression, including the magnitude of the compressive stress provided by the supporting tool, was proved to affect the formability in DSIF. Smith et al. [16] compared the deformation mechanics of SPIF and DSIF by performing FE analysis and found that the existence of the compression caused higher hydrostatic pressure and shear strains, which delayed the initiation and development of fracture, thus improving formability. Lu et al. [24] obtained the stress distribution in the contact areas, including the single-contact area and the dual-contact area, and found a phenomenon called Drop of Stress Triaxiality (DOST). Stress triaxiality suddenly dropped to a negative value in the dual-contact area. A smaller stress triaxiality meant less chance of damage development in the material, thus achieving better material formability, as shown in Fig. 34.

In the experiment conducted later, Lu et al. [24] investigated a wider range of the compressive force produced by the supporting tool in which the value of the supporting force was increased from 160 to 640 N. As shown in Fig. 35a, the maximum forming depth was increased considerably by about 50% at first when the supporting force was increased to 480 N; then, it started to decrease when a higher compressive force of 560 N was applied. It was explained that the extremely high compression effect between the sheet and the contacting tools caused surface damage and severe sheet stretching in the forming tool movement direction, which can be reflected by the mark left on the surface of the part, as shown in Fig. 35b.

3.1.2 Relative position of the tools

Adjusting the relative position of the two tools in DSIF will simultaneously change the division of the deformation zones, thus affecting the strain and stress distributions in the deforming sheet. Consequently, the forming limit can be influenced. As shown in Fig. 36, Lu et al. [24] found that under the supporting force of 480 N, the FLC for DSIF with tool shift was higher than that without tool shift.

3.2 Current investigation into the fracture mechanism of DSIF

Valoppi et al. [98] manufactured a double curved part using electricity-assisted DSIF and conducted fractography analysis of the fracture surface of the samples by using SEM. According to

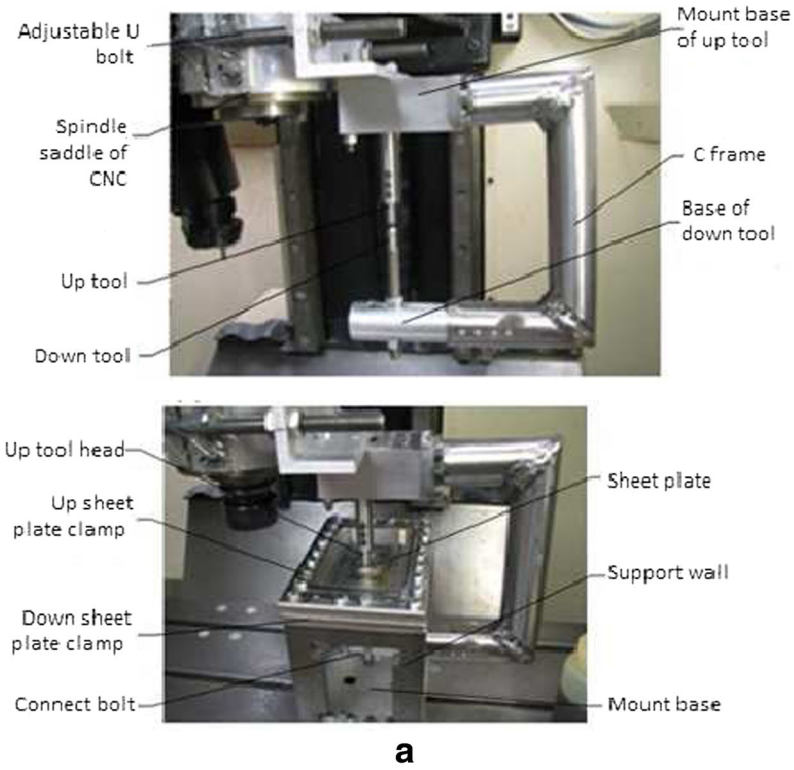

Fig. 32 DSIF equipment developed by the researchers: **a** C-frame mechanism [93]. **b** developed DSIF platform with two independently controlled tools [94], and **c** DSFI using a cooperating robot system [95]

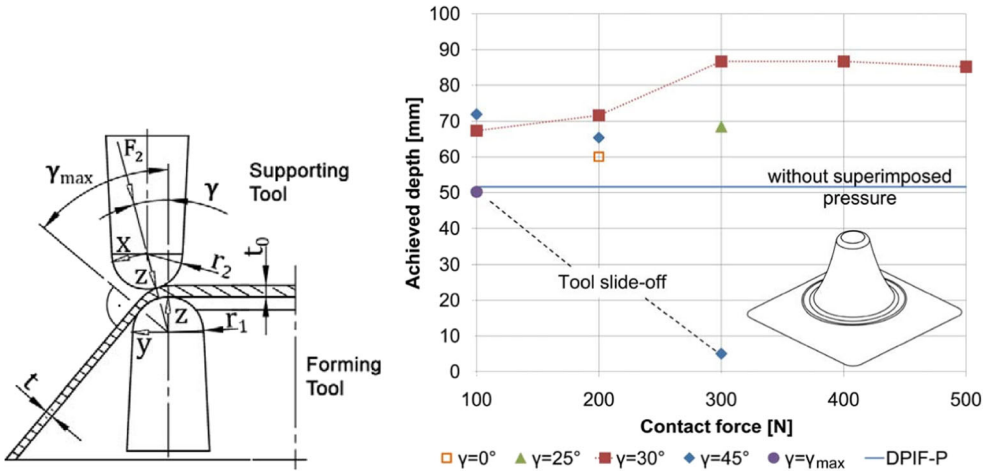

Fig. 33 Achieved depth of hyperbolic parts with varied contact force and shifting angle in DSIF [3]

their analysis, mode I fracture, namely tearing, was prone to occur in zone III due to its higher stress triaxiality and tapered thickness compared to that in zone I and zone II, while at the same time, the local bending and through-thickness-shear effect intensified the initiation of the crack on the outer surface in zone III, as shown in Fig. 37. The analysis was supported by the appearance and direction of dimples that appeared in the crack surface.

Lu et al. [24] observed the location and morphology of the fracture surface and claimed that they could be influenced by both the supporting force and the position of the tools. As shown in Fig. 38, tearing cracks were observed when different relative positions of the tools were applied. Cracks initiated in the single-contact zones, however, propagated in different directions. In Fig. 38a, the crack developed into the dual-contact zone while in Fig. 38b, the crack stayed in the single-contact zone, parallel to the tool movement direction. The authors concluded that the crack propagation in Fig. 38b was caused by the post-stretching of the forming tool. The relative position of the tools and magnitude of the supporting force applied changed the stress and strain distributions in the affected zones, leading to a different fracture behavior in DSIF.

4 Discussions and future research directions

Substantial work has been done on the deformation mechanism of the ISF process, especially for SPIF. Tearing of the testing material due to the existence of a stretching effect has been observed upon the fracture in ISF-formed parts. As summarized in Fig. 39, the deformation mechanism of ISF and material mechanical properties affect the initiation and propagation of the damage in the metal sheet during the process directly or indirectly. However, current research on fracture in ISF is more descriptive than explanative. Extensive observations on the fracture behavior of materials in ISF have been reported by the researchers without further consolidating explanations. An in-depth understanding on the facture mechanism has yet to be developed.

For SPIF, a common agreement regarding the location of the initiation of the fracture and the mechanism behind the transition between the necking-preceded fracture and rupture has yet to be established. The incomplete understanding regarding the fracture initiation location may be a result of the current persistent focus on the contact zone only while ignoring the areas around the contact. Extensive experimental

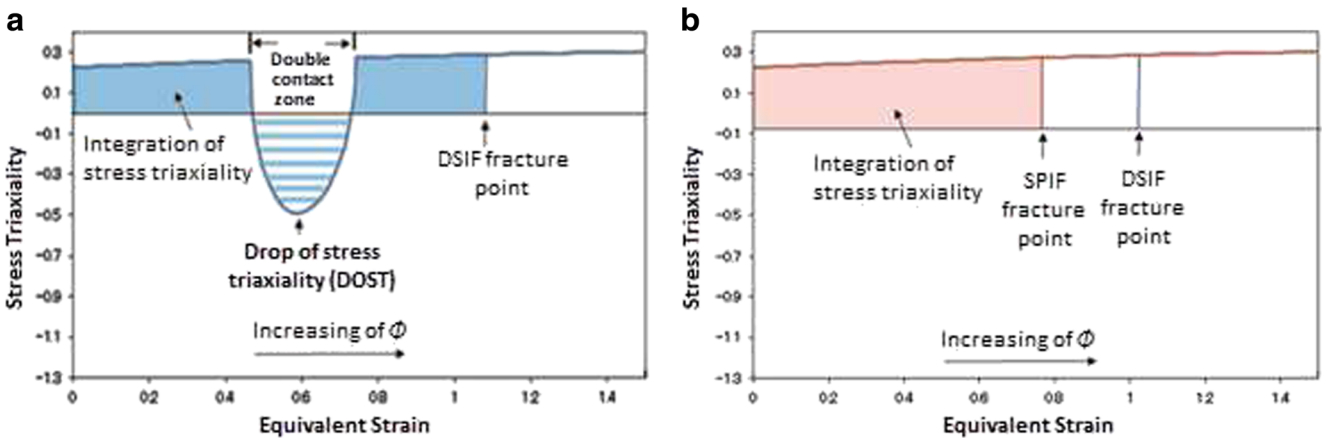

Fig. 34 Comparison of stress triaxiality variations with plastic strain **a** DSIF and **b** SPIF [24]

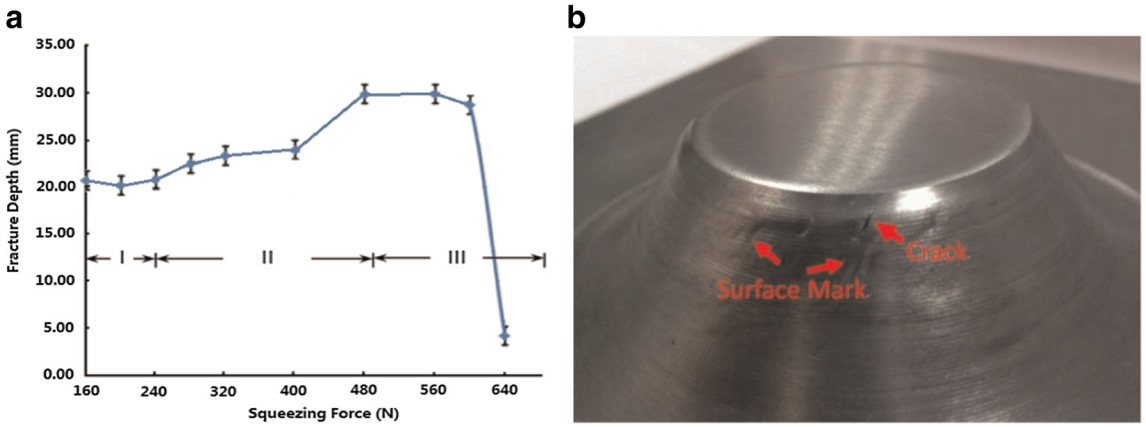

Fig. 35 Influence of supporting force on material formability in DSIF using material AA7075-T6 [24]: **a** the fracture depth of the cone shapes under varied supporting forces and **b** surface marks and cracks observed in the formed part

observations of the SPIF process may provide further insight for developing an in-depth understanding. Based on the evidence reported in various studies, the transition can be influenced by both the process parameters and material properties. In order to expand the understanding regarding how the transition occurs between the necking-initiated and fracture-initiated failures, a systematic investigation on the influence of the key factors including material properties, tool size, vertical step size, and feed rate on the initiation and development of the cracks in SPIF should be conducted in order to provide a full explanation of the phenomenon. The location of the crack should also be studied to facilitate a clear analysis of the material deformation. To develop a unified theory for the fracture of parts made by different materials under various loading conditions, further investigations are still required.

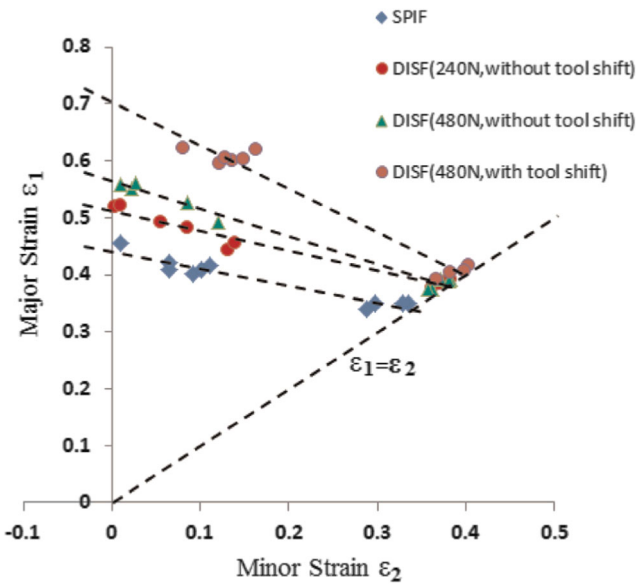

Fig. 36 Forming limits of DSIF with different relative locations between the master tool and the supporting tool [24]

While for DSIF, considering its complicated contact conditions, the difference between DSIF and SPIF may result in a significant difference between their fracture mechanisms, including the initiation and the development of the fracture. The existence of the compressive force brings another dimension into the loading conditions, and it is highly possible that the relative significance between the deformation mechanisms including stretching, bending, shearing, compression, and cyclic effects will shift as well, adding more possibilities of fracture location to the fracture mechanism in DSIF when subjected to different process parameters or for different materials. However, the investigation on the fracture behaviors and mechanism in DSIF is extremely limited, which compromises its process advantages. Despite its unique characteristics, DSIF is still considered as SPIF with superimposed compression. Limited materials have been tested and limited experiments have been conducted on DSIF, resulting in limited exposure of complex features of its deformation behavior. Similar to SPIF, the location of the crack initiation has not been confirmed in the reported studies. Without the evidence of the experimental results, the simulation and the theoretical analysis cannot be validated. The requirement of greater investment on the customization of the DSIF equipment may be blamed for the limited experimental work conducted.

To facilitate the design of the ISF process, a better prediction of the forming limit of ISF is required. Up to now, no generalized procedures for formability of ISF have been commonly agreed on due to the complexity of the ISF process, especially for the DSIF process. Although the prediction for the fracture in ISF is still not fully convincing by employing the traditional methods, the fracture-forming limit and the stress-based FLD have shown to be useful in fracture prediction in some reported studies. Further research using these methods for fracture prediction should be carried out on a wide selection of materials and process parameters.

For FE damage modeling of the ISF process, the selection of an accurate damage model is crucial to achieve accurate

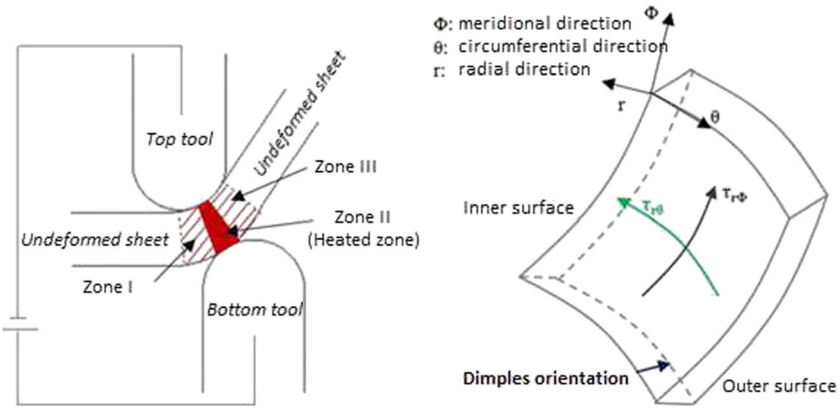

Fig. 37 Different deformation zones in DSIF [98]: **a** division of the deformation zones and **b** a schematic of the dimple direction with regard to sheet surfaces

results. Malcher et al. [99] assessed four commonly adopted isotropic damage models, including the GTN model, GTN model with shear mechanism enhancement, Lemaitre model [100], and Bai-Wierzbicki model [101], by comparing the simulation results obtained from the different damage models with the experimental results. Different geometries were designed to achieve a larger coverage of stress triaxiality in the uniaxial tensile tests. According to their findings, the GTN model with Xue's shear modification and the Lemaitre model presented better accuracy in predicting the damage location in the low-stress triaxiality zone than the Bai-Wierzbicki model while all the damage models achieved acceptable agreement with the experimental results in the high and moderate triaxiality zones. For ISF, the existence of the combination of multiple deformation modes makes it difficult to find a suitable damage model for the process. Furthermore, for DSIF, the stress triaxiality varies in different zones due to the complicated contact conditions, which makes it even more difficult to find a suitable damage model for the process to cover a wide range of stress triaxiality.

A simplified testing model representing the loading conditions of ISF would allow the development of in-depth understanding towards ISF facture mechanisms. For example, the influence of combined tension and bending on the enhanced formability of materials has been validated by Emmens and Van den Boogaard [21]. For DSIF, a modified tension-under-bending-and-compression test concept was proposed by Ai et al. [102] to investigate the combined effect of stretching, bending, compression, and cyclic effects on the material formability. While the deformation modes of ISF are properly

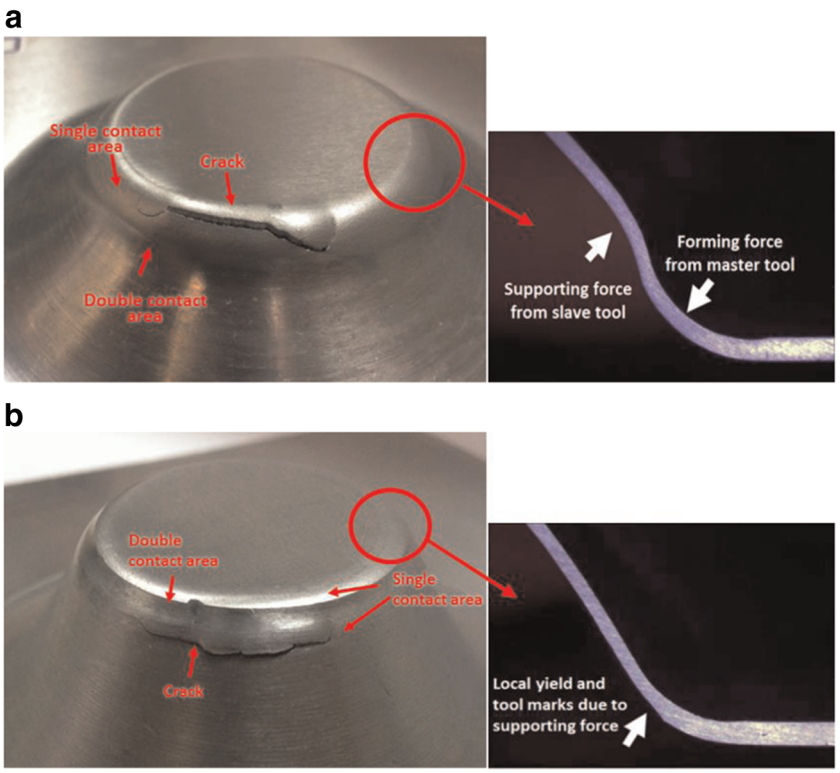

Fig. 38 Part fracture with different relative locations between the master tool and the supporting tool [24]: **a** without tool shift and **b** with tool shift

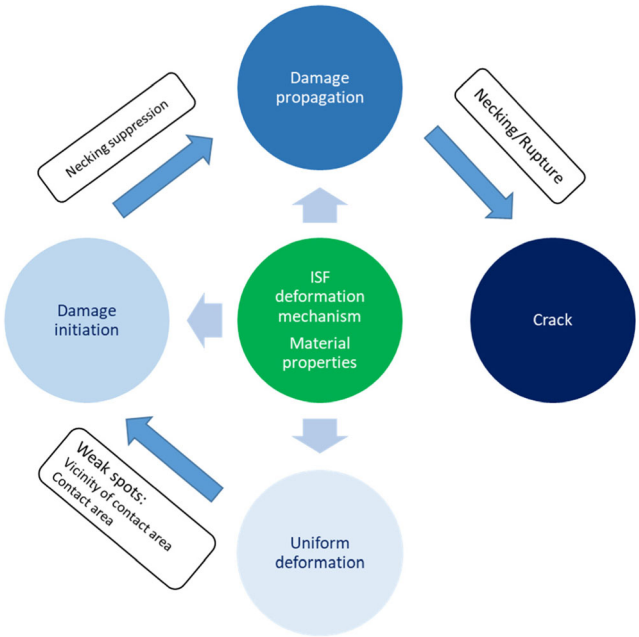

Fig. 39 Schematic of the fracture mechanism of ISF in current review

reflected in these tests, the geometric constraints in the ISF processes are not adequately represented. If the strain conditions and the geometric constraints are also considered in the tests, a better prediction of the damage initiation and propagation leading to fracture may be achieved.

5 Summary

This paper presents a complete review on investigation of material fracture in the ISF process, including SPIF and DSIF. Existing methods to predict the initiation of the fracture including FLC/FFLD, analytical methods, and damage modeling are compared in this review. Unique deformation characteristics contributing to the delay of facture in ISF are summarized. Two different types of fracture mechanisms including necking-initiated and fracture-initiated failures are observed in SPIF which makes the prediction of material fracture in ISF challenging.

This literature review shows that investigations on the fracture mechanism in ISF, especially DSIF, are very limited. Evidence provided by the published studies are scattered due to the fact that the majority of the experimental investigations focus only on the uniform material deformation in the ISF process without in-depth analysis of the material fracture behavior. Future research directions should focus on the material fracture behavior in ISF based on a systematic design of experimental tests taking both material properties and ISF process parameters into consideration. Damage modeling should focus on considering the complicated loading conditions in ISF to predict the material fracture. Appropriate damage models need to be developed to allow the material deformation modes and characteristics of the ISF process to be accurately modeled. An alternative way to investigate the complicated loading conditions in ISF is to develop simplified formability testing methods representing ISF in both deformation mechanics and geometric constraints.

Acknowledgements The first author would like to acknowledge the scholarship received from the Faculty of Engineering, The University of Sheffield, to support this research.

References

1. Edward L (1967) Apparatus and process for incremental dieless forming. Google Patents
2. Iseki H, Kato K, Sakamoto S (1989) Flexible and incremental sheet metal forming using a spherical roller. Proc 40th JJCTP 41:44
3. Meier H, Magnus C, Smukala V (2011) Impact of superimposed pressure on dieless incremental sheet metal forming with two moving tools. CIRP Ann Manuf Technol 60(1):327–330
4. Emmens W, Sebastiani G, van den Boogaard AH (2010) The technology of incremental sheet forming—a brief review of the history. J Mater Process Technol 210(8):981–997
5. Duflou JR, Habraken A-M, Cao J, Malhotra R, Bambach M, Adams D, Vanhove H, Mohammadi A, Jeswiet J (2017) Single point incremental forming: state-of-the-art and prospects. Int J Mater Form:1–31
6. Behera AK, de Sousa RA, Ingarao G, Oleksik V (2017) Single point incremental forming: an assessment of the progress and technology trends from 2005 to 2015. J Manuf Process 27:37–62
7. Li Y, Chen X, Liu Z, Sun J, Li F, Li J, Zhao G (2017) A review on the recent development of incremental sheet-forming process. Int J Adv Manuf Technol:1–24
8. Silva M, Martins P (2013) Two-point incremental forming with partial die: theory and experimentation. J Mater Eng Perform 22(4):1018–1027
9. Fan G, Sun F, Meng X, Gao L, Tong G (2010) Electric hot incremental forming of Ti-6Al-4V titanium sheet. Int J Adv Manuf Technol 49(9–12):941–947
10. Van Sy L, Thanh Nam N (2013) Hot incremental forming of magnesium and aluminum alloy sheets by using direct heating system. Proc Inst Mech Eng B J Eng Manuf 227(8):1099–1110
11. Ambrogio G, Filice L, Manco G (2008) Warm incremental forming of magnesium alloy AZ31. CIRP Ann Manuf Technol 57(1):257–260
12. Duflou J, Callebaut B, Verbert J, De Baerdemaeker H (2007) Laser assisted incremental forming: formability and accuracy improvement. CIRP Ann Manuf Technol 56(1):273–276
13. Duflou J, Callebaut B, Verbert J, De Baerdemaeker H (2008) Improved SPIF performance through dynamic local heating. Int J Mach Tools Manuf 48(5):543–549

14. Fang Y, Lu B, Chen J, Xu D, Ou H (2014) Analytical and experimental investigations on deformation mechanism and fracture behavior in single point incremental forming. J Mater Process Technol 214(8):1503–1515
15. Jackson K, Allwood J (2009) The mechanics of incremental sheet forming. J Mater Process Technol 209(3):1158–1174
16. Smith J, Malhotra R, Liu W, Cao J (2013) Deformation mechanics in single-point and accumulative double-sided incremental forming. Int J Adv Manuf Technol 69(5–8):1185–1201
17. Maqbool F, Bambach M (2018) Dominant deformation mechanisms in single point incremental forming (SPIF) and their effect on geometrical accuracy. Int J Mech Sci 136:279–292
18. Esmaeilpour R, Kim H, Park T, Pourboghrat F, Mohammed B (2017) Comparison of 3D yield functions for finite element simulation of single point incremental forming (SPIF) of aluminum 7075. Int J Mech Sci 133:544–554
19. Esmaeilpour R, Kim H, Park T, Pourboghrat F, Xu Z, Mohammed B, Abu-Farha F (2018) Calibration of Barlat Yld2004-18P yield function using CPFEM and 3D RVE for the simulation of single point incremental forming (SPIF) of 7075-O aluminum sheet. Int J Mech Sci 145:24–41
20. Lu B, Fang Y, Xu D, Chen J, Ou H, Moser N, Cao J (2014) Mechanism investigation of friction-related effects in single point incremental forming using a developed oblique roller-ball tool. Int J Mach Tools Manuf 85:14–29
21. Emmens W, Van den Boogaard A (2009) Incremental forming by continuous bending under tension—an experimental investigation. J Mater Process Technol 209(14):5456–5463
22. Gatea S, Ou H, McCartney G (2016) Review on the influence of process parameters in incremental sheet forming. Int J Adv Manuf Technol 87(1–4):479–499
23. McAnulty T, Jeswiet J, Doolan M (2017) Formability in single point incremental forming: a comparative analysis of the state of the art. CIRP J Manuf Sci Technol 16:43–54
24. Lu B, Fang Y, Xu D, Chen J, Ai S, Long H, Ou H, Cao J (2015) Investigation of material deformation mechanism in double side incremental sheet forming. Int J Mach Tools Manuf 93:37–48
25. Moser N, Zhang Z, Ren H, Ehmann K, Cao J (2016) An investigation into the mechanics of double-sided incremental forming using finite element methods. In: AIP Conference Proceedings, vol 1. AIP Publishing, p 070021
26. Anderson TL (2017) Fracture mechanics: fundamentals and applications. CRC press
27. Gupta P, Jeswiet J (2017) Observations on heat generated in single point incremental forming. Procedia Eng 183:161–167
28. Ai S, Lu B, Chen J, Long H, Ou H (2017) Evaluation of deformation stability and fracture mechanism in incremental sheet forming. Int J Mech Sci 124:174–184
29. Centeno G, Bagudanch I, Morales-Palma D, García-Romeu M, Gonzalez-Perez-Somarriba B, Martinez-Donaire A, Gonzalez-Perez L, Vallellano C (2017) Recent approaches for the manufacturing of polymeric cranial prostheses by incremental sheet forming. Procedia Eng 183:180–187
30. Zhang X, Wang J, Zhang S study on process parameters on single point incremental forming of PVC. In: Materials Science Forum, 2017
31. Shim M-S, Park J-J (2001) The formability of aluminum sheet in incremental forming. J Mater Process Technol 113(1):654–658
32. Martins P, Bay N, Skjødt M, Silva M (2008) Theory of single point incremental forming. CIRP Ann Manuf Technol 57(1): 247–252
33. Filice L, Fratini L, Micari F (2002) Analysis of material formability in incremental forming. CIRP Ann Manuf Technol 51(1):199–202
34. Fratini L, Ambrogio G, Di Lorenzo R, Filice L, Micari F (2004) Influence of mechanical properties of the sheet material on formability in single point incremental forming. CIRP Ann Manuf Technol 53(1):207–210
35. Keeler SP, Backofen WA (1963) Plastic instability and fracture in sheets stretched over rigid punches. Asm Trans Q 56(1):25–48
36. Goodwin GM (1968) Application of strain analysis to sheet metal forming problems in the press shop. SAE Trans:380–387
37. Banabic D (2000) Formability of metallic materials: plastic anisotropy, formability testing, forming limits. Springer Science & Business Media
38. Emmens W, van der Weijde D, van den Boogaard A (2009) The FLC, enhanced formability, and incremental sheet forming. In: Proceedings of the International Deep Drawing Research Group IDDRG 2009 International Conference, pp 1–3
39. Benedyk J, Parikh N, Stawarz D (1971) A method for increasing elongation values for ferrous and nonferrous sheet metals (ferrous and nonferrous sheet metals neck formation prevention for increasing elongation in tensile tests, using continuous plastic bending method). J Mater 6:16–29
40. Iseki H (2001) An approximate deformation analysis and FEM analysis for the incremental bulging of sheet metal using a spherical roller. J Mater Process Technol 111(1):150–154
41. Haque MZ, Yoon JW (2016) Stress based prediction of formability and failure in incremental sheet forming. Int J Mater Form 9(3): 413–421
42. Silva M, Skjødt M, Bay N, Martins P (2009) Revisiting single-point incremental forming and formability/failure diagrams by means of finite elements and experimentation. J Strain Anal Eng Des 44(4):221–234
43. Isik K, Silva M, Tekkaya A, Martins P (2014) Formability limits by fracture in sheet metal forming. J Mater Process Technol 214(8):1557–1565
44. Suresh K, Regalla SP (2014) Analysis of formability in single point incremental forming using finite element simulations. Procedia Mater Sci 6:430–435
45. Hussain G, Gao L (2007) A novel method to test the thinning limits of sheet metals in negative incremental forming. Int J Mach Tools Manuf 47(3):419–435
46. Young D, Jeswiet J (2004) Wall thickness variations in single-point incremental forming. Proc Inst Mech Eng B J Eng Manuf 218(11):1453–1459
47. Hussain G, Gao L, Hayat N, Ziran X (2009) A new formability indicator in single point incremental forming. J Mater Process Technol 209(9):4237–4242
48. Emmens W, Van den Boogaard A (2009) An overview of stabilizing deformation mechanisms in incremental sheet forming. J Mater Process Technol 209(8):3688–3695
49. Eyckens P, Van Bael A, Van Houtte P (2009) Marciniak–Kuczynski type modelling of the effect of through-thickness shear on the forming limits of sheet metal. Int J Plast 25(12):2249–2268
50. Eyckens P, Belkassem B, Henrard C, Gu J, Sol H, Habraken AM, Duflou JR, Van Bael A, Van Houtte P (2011) Strain evolution in the single point incremental forming process: digital image correlation measurement and finite element prediction. Int J Mater Form 4(1):55–71
51. Jeswiet J, Micari F, Hirt G, Bramley A, Duflou J, Allwood J (2005) Asymmetric single point incremental forming of sheet metal. CIRP Ann Manuf Technol 54(2):88–114
52. Liu R, Lu B, Xu D, Chen J, Chen F, Ou H, Long H (2015) Development of novel tools for electricity-assisted incremental sheet forming of titanium alloy. The International Journal of Advanced Manufacturing Technology:1–8
53. Ji Y, Park J (2008) Formability of magnesium AZ31 sheet in the incremental forming at warm temperature. J Mater Process Technol 201(1):354–358
54. Palumbo G, Brandizzi M (2012) Experimental investigations on the single point incremental forming of a titanium alloy

component combining static heating with high tool rotation speed. Mater Des 40:43–51
55. Kim Y, Park J (2002) Effect of process parameters on formability in incremental forming of sheet metal. J Mater Process Technol 130:42–46
56. Hussain G, Gao L, Zhang Z (2008) Formability evaluation of a pure titanium sheet in the cold incremental forming process. Int J Adv Manuf Technol 37(9):920–926
57. Huang G, Matlock D, Krauss G (1989) Martensite formation, strain rate sensitivity, and deformation behavior of type 304 stainless steel sheet. Metall Trans A 20(7):1239–1246
58. Picu R, Vincze G, Ozturk F, Gracio J, Barlat F, Maniatty A (2005) Strain rate sensitivity of the commercial aluminum alloy AA5182-O. Mater Sci Eng A 390(1):334–343
59. Smerd R, Winkler S, Salisbury C, Worswick M, Lloyd D, Finn M (2005) High strain rate tensile testing of automotive aluminum alloy sheet. Int J Impact Eng 32(1):541–560
60. Xu D, Wu W, Malhotra R, Chen J, Lu B, Cao J (2013) Mechanism investigation for the influence of tool rotation and laser surface texturing (LST) on formability in single point incremental forming. Int J Mach Tools Manuf 73:37–46
61. Buffa G, Campanella D, Fratini L (2013) On the improvement of material formability in SPIF operation through tool stirring action. Int J Adv Manuf Technol 66(9–12):1343–1351
62. Otsu M, Ichikawa T, Matsuda M, Takashima K (2011) Improvement of formability of magnesium alloy sheets by friction stir incremental forming. Steel Research International, Special Edition:537–541
63. Durante M, Formisano A, Langella A, Minutolo FMC (2009) The influence of tool rotation on an incremental forming process. J Mater Process Technol 209(9):4621–4626
64. Micari F (2004) Single point incremental forming: recent results. In: Seminar on Incremental forming
65. Skjødt M, Hancock MH, Bay N (2007) Creating helical tool paths for single point incremental forming. In: Key engineering materials. Trans Tech Publ, pp 583–590
66. Malhotra R, Reddy N, Cao J (2010) Automatic 3D spiral toolpath generation for single point incremental forming. J Manuf Sci Eng 132(6):061003
67. Lu B, Chen J, Ou H, Cao J (2013) Feature-based tool path generation approach for incremental sheet forming process. J Mater Process Technol 213(7):1221–1233
68. Huang Y, Cao J, Smith S, Woody B, Ziegert J, Li M (2008) Studies of size effect on the formability of a domed part in incremental forming. In: ASME 2008 International Manufacturing Science and Engineering Conference collocated with the 3rd JSME/ASME International Conference on Materials and Processing. American Society of Mechanical Engineers, pp 645–654
69. Silva M, Skjødt M, Martins PA, Bay N (2008) Revisiting the fundamentals of single point incremental forming by means of membrane analysis. Int J Mach Tools Manuf 48(1):73–83
70. Besson J (2010) Continuum models of ductile fracture: a review. Int J Damage Mech 19(1):3–52
71. Malhotra R, Xue L, Belytschko T, Cao J (2012) Mechanics of fracture in single point incremental forming. J Mater Process Technol 212(7):1573–1590
72. Mirnia MJ, Shamsari M (2017) Numerical prediction of failure in single point incremental forming using a phenomenological ductile fracture criterion. J Mater Process Technol 244:17–43
73. Guzmán CF, Yuan S, Duchêne L, Flores EIS, Habraken AM (2018) Damage prediction in single point incremental forming using an extended Gurson model. Int J Solids Struct 151:45–56
74. Wu S, Song N, Pires FA (2016) A comparative study of failure with incremental forming. In: Journal of physics: conference series, vol 3. IOP Publishing, p 032065
75. Gatea S, Ou H, Lu B, McCartney G (2017) Modelling of ductile fracture in single point incremental forming using a modified GTN model. Eng Fract Mech 186:59–79
76. Yue ZM, Chu XR, Gao J (2017) Numerical simulation of incremental sheet forming with considering yield surface distortion. Int J Adv Manuf Technol 92(5):1761–1768. https://doi.org/10.1007/s00170-017-0269-2
77. Silva M, Skjødt M, Atkins A, Bay N, Martins P (2008) Single-point incremental forming and formability—failure diagrams. J Strain Anal Eng Des 43(1):15–35
78. Hussain G, Gao L, Hayat N, Qijian L (2007) The effect of variation in the curvature of part on the formability in incremental forming: an experimental investigation. Int J Mach Tools Manuf 47(14):2177–2181
79. Dwivedi D, Kumar A, Priyadarshi S, Tandon P (2016) Numerical prediction of fracture in parts formed with incremental sheet forming process. Proceeding of AIMTDR:1061–1064
80. El-Sebaie M, Mellor P (1972) Plastic instability conditions in the deep-drawing of a circular blank of sheet metal. Int J Mech Sci 14(9):535–540
81. Silva MB, Nielsen PS, Bay N, Martins PA (2011) Failure mechanisms in single-point incremental forming of metals. Int J Adv Manuf Technol 56(9–12):893–903
82. Madeira T, Silva C, Silva M, Martins P (2015) Failure in single point incremental forming. Int J Adv Manuf Technol 80(9–12):1471–1479
83. Bambach M, Todorova M, Hirt G (2007) Experimental and numerical analysis of forming limits in CNC incremental sheet forming. In: Key engineering materials. Trans Tech Publ, pp 511–518
84. Emmens W, van den Boogaard AH (2010) Contact effects in bending affecting stress and formability. Int J Mater Form 3(1):1159–1162
85. Centeno G, Bagudanch I, Martínez-Donaire AJ, Garcia-Romeu ML, Vallellano C (2014) Critical analysis of necking and fracture limit strains and forming forces in single-point incremental forming. Mater Des 63:20–29
86. Morales D, Martinez A, Vallellano C, Garcia-Lomas F (2009) Bending effect in the failure of stretch-bend metal sheets. Int J Mater Form 2:813–816
87. Stoughton TB, Yoon JW (2011) A new approach for failure criterion for sheet metals. Int J Plast 27(3):440–459
88. Seong D, Haque M, Kim J, Stoughton T, Yoon J (2014) Suppression of necking in incremental sheet forming. Int J Solids Struct 51(15):2840–2849
89. Hadoush A, van den Boogaard AH, Emmens W (2011) A numerical investigation of the continuous bending under tension test. J Mater Process Technol 211(12):1948–1956
90. Barrett T, Kinsey B, Knezevic M, Korkolis Y (2017) Numerical and experimental investigation of formability enhancement during continuous-bending-under-tension (CBT) of AA6022-T4. Procedia Eng 207:1940–1945
91. Micari F, Ambrogio G, Filice L (2007) Shape and dimensional accuracy in single point incremental forming: state of the art and future trends. J Mater Process Technol 191(1):390–395
92. Malhotra R, Cao J, Ren F, Kiridena V, Xia ZC, Reddy N (2011) Improvement of geometric accuracy in incremental forming by using a squeezing toolpath strategy with two forming tools. J Manuf Sci Eng 133(6):061019
93. Wang Y, Huang Y, Cao J, Reddy NV (2008) Experimental study on a new method of double side incremental forming. In: Proceedings of the 2008 International Manufacturing Science and Engineering Conference. MSEC
94. Malhotra R, Cao J, Beltran M, Xu D, Magargee J, Kiridena V, Xia ZC (2012) Accumulative-DSIF strategy for enhancing process

capabilities in incremental forming. CIRP Ann Manuf Technol 61(1):251–254
95. Meier H, Smukala V, Dewald O, Zhang J (2007) Two point incremental forming with two moving forming tools. In: Key engineering materials. Trans Tech Publ, pp 599–605
96. Xu R, Ren H, Zhang Z, Malhotra R, Cao J (2014) A mixed toolpath strategy for improved geometric accuracy and higher throughput in double-sided incremental forming. In: ASME 2014 international manufacturing science and engineering conference collocated with the JSME 2014 international conference on materials and processing and the 42nd North American manufacturing research conference. American Society of Mechanical Engineers, p V002T002A082-V002T002A082
97. Smith L, Averill R, Lucas J, Stoughton T, Matin P (2003) Influence of transverse normal stress on sheet metal formability. Int J Plast 19(10):1567–1583
98. Valoppi B, Zhang Z, Deng M, Ghiotti A, Bruschi S, Ehmann KF, Cao J (2017) On the fracture characterization in double-sided incremental forming of Ti6Al4V sheets at elevated temperatures. Procedia Manuf 10:407–416
99. Malcher L, Pires FA, De Sá JC (2012) An assessment of isotropic constitutive models for ductile fracture under high and low stress triaxiality. Int J Plast 30:81–115
100. Lemaitre J (1985) A continuous damage mechanics model for ductile fracture. J Eng Mater Technol 107(1):83–89
101. Bai Y, Wierzbicki T (2008) A new model of metal plasticity and fracture with pressure and lode dependence. Int J Plast 24(6): 1071–1096
102. Ai S, Lu B, Long H (2017) An analytical study of new material test method for tension under bending and compression in double side incremental forming. Procedia Eng 207:1982–1987